Alleviating Sensor Position Error in Source Localization Using Calibration Emitters at Inaccurate Locations

Le Yang, *Student Member, IEEE*, and K. C. Ho, *Fellow, IEEE*

***Abstract*—A previous study shows that the use of a calibration emitter whose position is known exactly can significantly reduce the loss in time differences of arrival (TDOA) based source localization accuracy when the available sensor positions have random errors. This paper extends the previous work to a more practical scenario where the exact position of a calibration emitter is not known. By modeling the calibration position error as additive Gaussian noise, the amount of reduction in localization accuracy due to calibration position error is derived through Cramér–Rao lower bound (CRLB) analysis. In addition, the analysis also affirms the previous studies on Bayesian sensor network localization that it remains possible to improve the localization accuracy even if the calibration position is completely unknown. Next, a performance analysis illustrates that the penalty could be very high if one simply pretends the calibration position is accurate and ignores its error. A closed-form solution is then developed by accounting for the calibration position error and it is proved analytically to reach the CRLB accuracy when the sensor and calibration position errors are small relative to the distance between the calibration emitter and the sensor. Finally, the results are generalized to the case where multiple calibration emitters are available. When deploying multiple calibration emitters, although their positions may not be known exactly, we show that it is possible to completely eliminate the sensor position error and recover the best localization accuracy that is limited by the measurement noise in TDOAs only. All the theoretical developments are corroborated by simulations.**

***Index Terms*—Calibration, localization, sensor position error, time difference of arrival (TDOA).**

I. Introduction

PASSIVE source localization has been the focus of considerable research efforts, due to its usefulness in various applications including sonar [1], radar [2] and more recently, sensor networks [3]–[6] and microphone array [7]. The localization task is usually accomplished using a two-step approach. In the first step, certain signal parameters, such as received signal strengths (RSS), time of arrivals (TOAs) and time differences of arrival (TDOAs), are extracted from the source emissions received at an array of spatially-distributed sensors. Then, in the second step, the source position is estimated by solving a set of non-linear equations defined by the signal parameters obtained in the first step. In this paper, we restrict our attention to identifying the position of a single stationary source from TDOAs.

A large number of TDOA localization algorithms are available in literature. Some algorithms obtain the source location estimate by solving the likelihood function in an iterative fashion [8]–[10]. A main drawback of these iterative solutions is that they require good initial solution guesses close to the true solution to begin with and may suffer from local convergence problem. Closed-form localization algorithms were developed for the purpose of overcoming this drawback [11]–[16]. They do not need initial position estimate and are computationally more attractive.

The performance of a localization algorithm depends heavily on the availability of accurate sensor positions. When the sensor positions are known precisely, most of these algorithms can attain the Cramér–Rao lower bound (CRLB) accuracy under certain signal-to-noise ratio (SNR) conditions. On the other hand, when the sensor position error is present, the localization accuracy of these methods would be significantly degraded and no longer reach the corresponding CRLB performance [17]. By explicitly taking the statistics of the sensor position error into account, [17] has developed an improved solution. Although such a solution can achieve the CRLB performance, the localization accuracy is in general much worse than the one when the sensor position error is absent [17].

Recently, Ho and Yang [18] investigated the use of a single calibration emitter whose position is known exactly to reduce the loss in localization accuracy due to the uncertainty in sensor positions. They showed through CRLB analysis that the introduction of a calibration emitter could provide significant performance gain. They also derived a novel closed-form solution that first utilizes the calibration TDOA measurements to improve the sensor positions and then applies the updated sensor positions to obtain a better source location estimate. The method was shown analytically to reach the CRLB accuracy before the thresholding effect occurs when the source is distant from the sensor array or when the SNR is sufficiently high.

This paper extends the work in [18] to a more realistic situation where the exact location of the calibration emitter is not available. Inaccurate knowledge on the calibration emitter location occurs quite often in practice. An example is that the calibration emitter is on a moving platform (such as a land vehicle or an unmanned aerial vehicle (UAV)) whose position is not able to be obtained precisely. Another example is that the emitter for calibration is unintentional, meaning that it is an unknown emitter whose position was previously estimated and hence the

Manuscript received July 25, 2008; accepted June 19, 2009. First published July 31, 2009; current version published December 16, 2009. The associate editor coordinating the review of this manuscript and approving it for publication was Dr. Brian M. Sadler.

The authors are with the Department of Electrical and Computer Engineering, University of Missouri, Columbia, MO 65211 USA (e-mail: lyx35@mail.mizzou.edu; hod@missouri.edu).

Digital Object Identifier 10.1109/TSP.2009.2028947

calibration emitter position is subject to estimation error. The amount of calibration position error would likely be smaller than the sensor position error if the calibration emitter is intentional, but could be much larger than the sensor position error if it is unintentional. The purpose of this paper is to address the effect of inaccurate calibration position on the source localization accuracy, and how to reach the optimum performance.

This paper also advances the previous work [18] by investigating the use of multiple calibration emitters to further improve the source location estimate. The motivation comes from the analysis result in [18] that a single calibration emitter is not able to completely remove the degradation in source localization accuracy due to sensor position errors. Provided that we have the luxury to deploy multiple calibration emitters, we are interested in determining whether the effect of sensor position errors can be fully eliminated and how many calibration emitters are needed to achieve this purpose.

The purpose of this paper is to investigate 1) how the calibration position error affects the source localization accuracy and how much we can tolerate the error so that the calibration emitter can still improve performance, 2) how sensitive the source localization accuracy is to the calibration position error if we simply ignore it, 3) how to take the statistical knowledge of the calibration position error into account, if needed, to obtain a better source location estimate, and 4) how to exploit multiple calibration emitters to improve the source localization accuracy, and the possibility of completely removing the effect of sensor position errors. To address item 1), CRLB analysis will be used. We show that the calibration position error degrades the source localization accuracy in the same manner as increasing the calibration TDOA noise and the exact amount of performance degradation is also derived. In the extreme case where the calibration position is completely not known, the analysis indicates that the calibration emitter remains to be able to improve the source localization accuracy. The CRLB analysis confirms the previous study on Bayesian sensor network localization that using calibration emitter, in spite of the presence of calibration position error, offers better source localization accuracy. The approach to investigate the second item is through analyzing the mean-square error (MSE) matrix of the source location estimate generated by a pseudo maximum likelihood (ML) estimator that assumes the calibration emitter position is exact but indeed has error. The result infers that the source localization accuracy is very sensitive to the noise in the calibration emitter position, especially when the calibration emitter is close to the sensor array, and hence the calibration position error cannot be ignored. The development of the third item is based on the algorithm in [18]. The statistics of the position errors in both the receiving sensors and the calibration emitter are exploited to come up with an algebraic closed-form solution. The new solution is shown analytically to achieve the CRLB accuracy under some mild conditions. Based on the understandings and insights obtained from items 1) to 3), we then proceed to study the source localization accuracy when multiple calibration emitters are available. We show through CRLB study that it is possible to completely eliminate the effect of sensor position errors on the source location estimate by properly exploring multiple calibration emitters. Generalization of the proposed closed-form solution to the localization scenario with arbitrary number of calibration emitters is summarized, together with a sketch of the proof that the accuracy of the generalized solution attains the CRLB under similar conditions as in the single calibration emitter case.

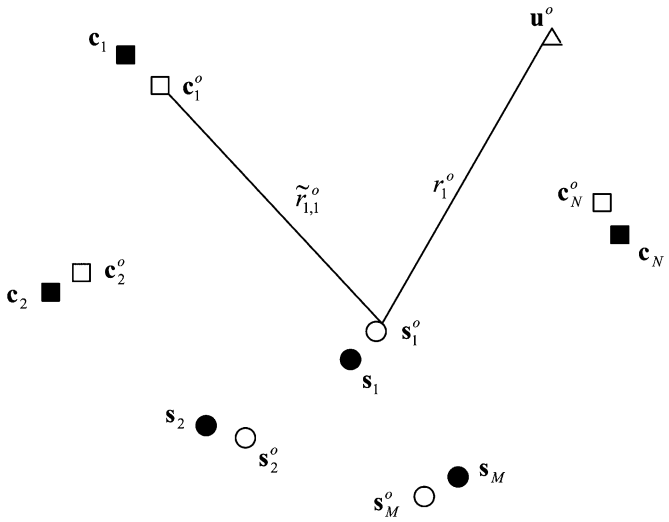

Fig. 1. Source localization scenario. The open circles represent the actual sensor positions that are not known and the solid circles are the available sensor positions that are erroneous. The triangle denotes the unknown source whose location is to be estimated. The open squares are the true calibration emitter positions that are not known and the solid squares are the available calibration emitter positions that are inaccurate.

The paper uses bold face lower case letters to represent column vectors and bold face upper case letters to denote matrices. If $(*)$ contains noise, $(*)^o$ is used to denote the true value of $(*)$. The symbols and notations used in this paper are summarized in Table II of Appendix I for quick reference.

We organize the paper as follows. In Section II, the localization scenario is described. The CRLB analysis is performed in Section III. The study of source location MSE when ignoring the calibration position error is examined in Section IV. Section V presents the new algebraic closed-form solution and its performance analysis. Sections III to V simplifies the illustration by considering a single calibration emitter. Section VI extends the results in the previous sections to TDOA localization using multiple calibration emitters. Simulation results are provided in Section VII to corroborate the theoretical derivations. Section VIII concludes the paper.

II. Localization Scenario

Fig. 1 illustrates the localization scenario examined in this paper. An array of M sensors at positions $\mathbf{s}_i^o = [x_{s,i}^o, y_{s,i}^o, z_{s,i}^o]^T$, $i = 1, 2, \ldots, M$, is used to determine the location of a stationary source whose unknown position is denoted by $\mathbf{u}^o = [x_u^o, y_u^o, z_u^o]^T$. The sensors receive the signal from the unknown source and the TDOAs of the source signal with respect to a reference sensor are obtained. The sensors also receive the signals from N calibration emitters located at $\mathbf{c}_j^o = [x_{c,j}^o, y_{c,j}^o, z_{c,j}^o]^T$, $j = 1, 2, \ldots, N$. For each calibration emitter, a set of calibration TDOAs is obtained. The location of the unknown source is to be identified by TDOA positioning.

Unlike the traditional localization scenario where the receiving sensor positions are known exactly, here only the noisy sensor positions $\mathbf{s}_i$ are available. They are modeled as [17], [18]

$$\mathbf{s}_i = \mathbf{s}_i^o + \mathbf{\Psi}_i, \quad i = 1, 2, \ldots, M \tag{1}$$

where $\mathbf{\Psi}_i$ is the position error in $\mathbf{s}_i$. For notation simplicity, we collect the available sensor positions to form the $3M \times 1$ sensor position vector $\mathbf{s} = [\mathbf{s}_1^T, \mathbf{s}_2^T, \ldots, \mathbf{s}_M^T]^T = \mathbf{s}^o + \mathbf{\Psi}$, where $\mathbf{s}^o = [\mathbf{s}_1^{oT}, \mathbf{s}_2^{oT}, \ldots, \mathbf{s}_M^{oT}]^T$ and $\mathbf{\Psi} = [\mathbf{\Psi}_1^T, \mathbf{\Psi}_2^T, \ldots, \mathbf{\Psi}_M^T]^T$. The sensor position error vector $\mathbf{\Psi}$ is assumed to be a zero mean Gaussian random vector with covariance matrix $\mathbf{Q}_\beta$.

The purpose of using calibration emitters is to reduce the effect of sensor position errors. Different from the previous work [18], the exact positions of calibration emitters are not known in this study. The calibration emitter locations $\mathbf{c}_j$ available to a localization algorithm are modeled as

$$\mathbf{c}_j = \mathbf{c}_j^o + \mathbf{e}_j, \quad j = 1, 2, \ldots, N \tag{2}$$

where $\mathbf{e}_j$ is the position error of the calibration emitter j. Again, collecting $\mathbf{c}_j$ to form a vector yields $\mathbf{c} = \mathbf{c}^o + \mathbf{e}$, where $\mathbf{c} = [\mathbf{c}_1^T, \mathbf{c}_2^T, \ldots, \mathbf{c}_N^T]^T$, $\mathbf{c}^o = [\mathbf{c}_1^{oT}, \mathbf{c}_2^{oT}, \ldots, \mathbf{c}_N^{oT}]^T$ and $\mathbf{e}$ is a $3N \times 1$ zero mean Gaussian random vector with covariance matrix $\mathbf{Q}_e$.

We shall denote the TDOA between sensor pair i and 1 from the unknown source as d_{i1}, and that from the jth calibration emitter as $\tilde{d}_{i1,j}$, where $i = 2, 3, \ldots, M$, $j = 1, 2, \ldots, N$ and sensor 1 is the reference sensor. Multiplying the TDOAs by the signal propagation speed v yields the range difference of arrival (RDOA) measurements

$$r_{i1} = v \cdot d_{i1} = r_{i1}^o + n_{i1} \tag{3a}$$

$$\tilde{r}_{i1,j} = v \cdot \tilde{d}_{i1,j} = \tilde{r}_{i1,j}^o + \tilde{n}_{i1,j} \tag{3b}$$

where n_{i1} and $\tilde{n}_{i1,j}$ denote the RDOA noises and they are v times the TDOA noises. The true RDOA r_{i1}^o is equal to the difference between the ranges of the unknown source to the two sensors, i.e.,

$$r_{i1}^o = r_i^o - r_1^o = \|\mathbf{u}^o - \mathbf{s}_i^o\| - \|\mathbf{u}^o - \mathbf{s}_1^o\| \tag{4}$$

where $\| \star \|$ is the Euclidean norm. The true RDOA $\tilde{r}_{i1,j}^o$ from the jth calibration emitter can be expressed in a similar form as

$$\tilde{r}_{i1,j}^o = \tilde{r}_{i,j}^o - \tilde{r}_{1,j}^o = \|\mathbf{c}_j^o - \mathbf{s}_i^o\| - \|\mathbf{c}_j^o - \mathbf{s}_1^o\|. \tag{5}$$

For notation simplicity, we shall represent the RDOA measurements from the unknown source by the vector $\mathbf{r} = [r_{21}, r_{31}, \ldots, r_{M1}]^T = \mathbf{r}^o + \mathbf{n}$, where $\mathbf{r}^o = [r_{21}^o, r_{31}^o, \ldots, r_{M1}^o]^T$, and those from the N calibration emitters as $\tilde{\mathbf{r}} = [\tilde{r}_{21,1}, \tilde{r}_{31,1}, \ldots, \tilde{r}_{M1,1}, \tilde{r}_{21,2}, \ldots, \tilde{r}_{M1,N}]^T = \tilde{\mathbf{r}}^o + \tilde{\mathbf{n}}$, where $\tilde{\mathbf{r}}^o = [\tilde{r}_{21,1}^o, \tilde{r}_{31,1}^o, \ldots, \tilde{r}_{M1,1}^o, \tilde{r}_{21,2}^o, \ldots, \tilde{r}_{M1,N}^o]^T$. $\mathbf{n}$ and $\tilde{\mathbf{n}}$ are modeled as zero mean Gaussian random vectors with covariance matrices $\mathbf{Q}_\alpha$ and $\mathbf{Q}_c$. The noise vectors $\mathbf{\Psi}$, $\mathbf{e}$, $\mathbf{n}$ and $\tilde{\mathbf{n}}$ are assumed to be independent with one another but the elements within each noise vector can be correlated. In other words, the covariance matrices of these noise vectors are not confined to diagonal matrices. The noise covariance matrices $\mathbf{Q}_\beta$ for sensor positions, $\mathbf{Q}_e$ for calibration positions, $\mathbf{Q}_\alpha$ for unknown source RDOAs and $\mathbf{Q}_c$ for calibration RDOAs are assumed to be known *a priori*.

The localization task considered here can be viewed as a special case of the Bayesian sensor network localization problem [19], [20]. In this perspective, the problem we address is to estimate from TDOA measurements the position of a source with non-informative prior using a sensor network composed of receiving sensors and transmitting (calibration) sensors whose positions are described by prior distributions.

For ease of illustration and comparison with previous results in [18], we shall consider using a single calibration emitter (i.e., $N = 1$) for locating the unknown source in Sections III to V. In such a case, $\mathbf{c} = \mathbf{c}_1$, $\mathbf{e} = \mathbf{e}_1$, $\tilde{\mathbf{r}} = [\tilde{r}_{21,1}, \tilde{r}_{31,1}, \ldots, \tilde{r}_{M1,1}]^T$, $\mathbf{Q}_e$ is 3×3 and $\mathbf{Q}_c$ is $(M-1) \times (M-1)$. The CRLB result and the localization algorithm developed for the single calibration emitter case will be generalized to the localization scenario with multiple calibration emitters in Section VI.

III. CRLB Analysis

The CRLB results presented in this section are valid only if the noises in the sensor and calibration emitter positions are Gaussian and their covariance matrices are known. These conditions may not be satisfied, depending on the scenarios encountered. Nevertheless, Gaussian and known noise models allow us to simplify the derivation and gain insights. In some cases, the distributions of the sensor and calibration position errors may come from some prior information, as described in [19], [20]. In other cases, they could come from the algorithm used to estimate the sensor and calibration emitter positions. For instance, the ML estimator provides parameter vector estimate that has asymptotically Gaussian distribution with its covariance matrix equal to the CRLB [21]. We also would like to mention that the study here using only CRLBs does not address the possible estimator if the sensor and calibration positions have nonzero mean errors. The effect of estimator bias is a topic for future study.

Under the localization scenario described in Section II, besides the source location $\mathbf{u}^o$, both the sensor position vector $\mathbf{s}^o$ and the calibration position vector $\mathbf{c}^o$ are not known. From our models (1) for the sensor positions and (2) for the calibration emitter locations, $\mathbf{s}^o$ and $\mathbf{c}^o$ are fixed and the deterministic CRLB formulation is used. The CRLB of $\mathbf{u}^o$ is evaluated through the use of the composite unknown parameter vector $\boldsymbol{\phi} = [\mathbf{u}^{oT}, \mathbf{s}^{oT}, \mathbf{c}^{oT}]^T$. Because $\mathbf{r}$, $\tilde{\mathbf{r}}$, $\mathbf{s}$ and $\mathbf{c}$ are Gaussian distributed and independent with one another, the logarithm of the probability density function of the data vector $\mathbf{v} = [\mathbf{r}^T, \tilde{\mathbf{r}}^T, \mathbf{s}^T, \mathbf{c}^T]^T$ is

$$\begin{aligned} \ln p(\mathbf{v}; \boldsymbol{\phi}) = K &- \frac{1}{2}(\mathbf{r} - \mathbf{r}^o)^T \mathbf{Q}_\alpha^{-1} (\mathbf{r} - \mathbf{r}^o) \\ &- \frac{1}{2}(\tilde{\mathbf{r}} - \tilde{\mathbf{r}}^o)^T \mathbf{Q}_c^{-1} (\tilde{\mathbf{r}} - \tilde{\mathbf{r}}^o) \\ &- \frac{1}{2}(\mathbf{s} - \mathbf{s}^o)^T \mathbf{Q}_\beta^{-1} (\mathbf{s} - \mathbf{s}^o) \\ &- \frac{1}{2}(\mathbf{c} - \mathbf{c}^o)^T \mathbf{Q}_e^{-1} (\mathbf{c} - \mathbf{c}^o) \end{aligned} \tag{6}$$

where K is a constant that does not depend on the unknowns. Applying partial derivatives with respect to $\boldsymbol{\phi}$ twice, negating

the sign and taking expectation give the Fisher information matrix (FIM)

$$\text{FIM} = \begin{bmatrix} \mathbf{X} & \mathbf{Y} & \mathbf{O} \\ \mathbf{Y}^T & \mathbf{Z} & \mathbf{R}^T \\ \mathbf{O} & \mathbf{R} & \mathbf{P} \end{bmatrix} \tag{7}$$

where

$$\mathbf{X}_{3\times 3} = -E\left[\frac{\partial^2 \ln p}{\partial \mathbf{u}^o \partial \mathbf{u}^{oT}}\right] = \left(\frac{\partial \mathbf{r}^o}{\partial \mathbf{u}^o}\right)^T \mathbf{Q}_\alpha^{-1}\left(\frac{\partial \mathbf{r}^o}{\partial \mathbf{u}^o}\right) \tag{8a}$$

$$\mathbf{Y}_{3\times 3M} = -E\left[\frac{\partial^2 \ln p}{\partial \mathbf{u}^o \partial \mathbf{s}^{oT}}\right] = \left(\frac{\partial \mathbf{r}^o}{\partial \mathbf{u}^o}\right)^T \mathbf{Q}_\alpha^{-1}\left(\frac{\partial \mathbf{r}^o}{\partial \mathbf{s}^o}\right) \tag{8b}$$

$$\begin{aligned}\mathbf{Z}_{3M\times 3M} &= -E\left[\frac{\partial^2 \ln p}{\partial \mathbf{s}^o \partial \mathbf{s}^{oT}}\right] \\ &= \mathbf{Q}_\beta^{-1} + \left(\frac{\partial \mathbf{r}^o}{\partial \mathbf{s}^o}\right)^T \mathbf{Q}_\alpha^{-1}\left(\frac{\partial \mathbf{r}^o}{\partial \mathbf{s}^o}\right) \\ &\quad + \left(\frac{\partial \tilde{\mathbf{r}}^o}{\partial \mathbf{s}^o}\right)^T \mathbf{Q}_c^{-1}\left(\frac{\partial \tilde{\mathbf{r}}^o}{\partial \mathbf{s}^o}\right)\end{aligned} \tag{8c}$$

$$\mathbf{R}_{3\times 3M} = -E\left[\frac{\partial^2 \ln p}{\partial \mathbf{c}^o \partial \mathbf{s}^{oT}}\right] = \left(\frac{\partial \tilde{\mathbf{r}}^o}{\partial \mathbf{c}^o}\right)^T \mathbf{Q}_c^{-1}\left(\frac{\partial \tilde{\mathbf{r}}^o}{\partial \mathbf{s}^o}\right) \tag{8d}$$

$$\begin{aligned}\mathbf{P}_{3\times 3} &= -E\left[\frac{\partial^2 \ln p}{\partial \mathbf{c}^o \partial \mathbf{c}^{oT}}\right] \\ &= \mathbf{Q}_e^{-1} + \left(\frac{\partial \tilde{\mathbf{r}}^o}{\partial \mathbf{c}^o}\right)^T \mathbf{Q}_c^{-1}\left(\frac{\partial \tilde{\mathbf{r}}^o}{\partial \mathbf{c}^o}\right)\end{aligned} \tag{8e}$$

and $\mathbf{O}$ is a 3×3 zero matrix. Let $\boldsymbol{\rho}_{\mathbf{a},\mathbf{b}} = (\mathbf{a}-\mathbf{b})/\|\mathbf{a}-\mathbf{b}\|$ be the unit vector from $\mathbf{b}$ to $\mathbf{a}$. From (4) and (5), the $(i-1)$th rows, $i = 2,3,\ldots,M$, of $(\partial \mathbf{r}^o/\partial \mathbf{u}^o)$, $(\partial \mathbf{r}^o/\partial \mathbf{s}^o)$, $(\partial \tilde{\mathbf{r}}^o/\partial \mathbf{c}^o)$ and $(\partial \tilde{\mathbf{r}}^o/\partial \mathbf{s}^o)$ are

$$\left(\frac{\partial r_{i1}^o}{\partial \mathbf{u}^o}\right)^T = \left[\boldsymbol{\rho}_{\mathbf{u}^o,\mathbf{s}_i^o}^T - \boldsymbol{\rho}_{\mathbf{u}^o,\mathbf{s}_1^o}^T\right] \tag{9a}$$

$$\left(\frac{\partial r_{i1}^o}{\partial \mathbf{s}^o}\right)^T = \left[\boldsymbol{\rho}_{\mathbf{u}^o,\mathbf{s}_1^o}^T, \underbrace{\mathbf{0}^T}_{1\times 3(i-2)}, -\boldsymbol{\rho}_{\mathbf{u}^o,\mathbf{s}_i^o}^T, \underbrace{\mathbf{0}^T}_{1\times 3(M-i)}\right] \tag{9b}$$

$$\left(\frac{\partial \tilde{r}_{i1,1}^o}{\partial \mathbf{c}^o}\right)^T = \left[\boldsymbol{\rho}_{\mathbf{c}^o,\mathbf{s}_i^o}^T - \boldsymbol{\rho}_{\mathbf{c}^o,\mathbf{s}_1^o}^T\right] \tag{9c}$$

$$\left(\frac{\partial \tilde{r}_{i1,1}^o}{\partial \mathbf{s}^o}\right)^T = \left[\boldsymbol{\rho}_{\mathbf{c}^o,\mathbf{s}_1^o}^T, \underbrace{\mathbf{0}^T}_{1\times 3(i-2)}, -\boldsymbol{\rho}_{\mathbf{c}^o,\mathbf{s}_i^o}^T, \underbrace{\mathbf{0}^T}_{1\times 3(M-i)}\right]. \tag{9d}$$

The CRLB of $\boldsymbol{\phi}$, denoted by $\text{CRLB}(\boldsymbol{\phi})$, is the inverse of the FIM. The upper-left three-by-three block of $\text{CRLB}(\boldsymbol{\phi})$ is the CRLB of the unknown source position $\mathbf{u}^o$ and it will be denoted as $\text{CRLB}(\mathbf{u}^o)_c$. Through applying partitioned matrix inversion formula [22] twice, Appendix II shows that

$$\begin{aligned}\text{CRLB}(\mathbf{u}^o)_c = \mathbf{X}^{-1} + \mathbf{X}^{-1}\mathbf{Y}(\mathbf{Z} - \mathbf{Y}^T\mathbf{X}^{-1}\mathbf{Y} \\ - \mathbf{R}^T\mathbf{P}^{-1}\mathbf{R})^{-1}\mathbf{Y}^T\mathbf{X}^{-1}.\end{aligned} \tag{10}$$

$\mathbf{X}^{-1}$ is the CRLB of $\mathbf{u}^o$ when the sensor position error is absent [17] and will be denoted as $\text{CRLB}(\mathbf{u}^o)$. The second term in the above equation is the aggregation of the increase in CRLB due to the sensor and calibration position errors. The trace of $\text{CRLB}(\mathbf{u}^o)_c$ is the minimum possible localization MSE that any unbiased estimator can achieve.

In the rest of this section, we shall perform a comprehensive analysis on the CRLB of the source location given in (10). Specifically, Section III-A examines the increase in CRLB resulted from inaccurate calibration emitter position for the purpose of understanding the effect of calibration position error on the source localization accuracy. In Section III-B, we study the performance improvement due to the use of a calibration emitter with position error over the case where the calibration emitter is not utilized. This section ends with some numerical examples in Section III-C to illustrate the obtained CRLB results.

A. Performance Degradation From Calibration Position Error

We shall contrast $\text{CRLB}(\mathbf{u}^o)_c$, the CRLB with calibration position error, with $\text{CRLB}(\mathbf{u}^o)_{c^o}$, the CRLB without calibration position error. $\text{CRLB}(\mathbf{u}^o)_{c^o}$ is given in (11) of [18] as

$$\text{CRLB}(\mathbf{u}^o)_{c^o} = \mathbf{X}^{-1} + \mathbf{X}^{-1}\mathbf{Y}(\mathbf{Z} - \mathbf{Y}^T\mathbf{X}^{-1}\mathbf{Y})^{-1}\mathbf{Y}^T\mathbf{X}^{-1}. \tag{11}$$

Comparing (10) with (11) indicates that the calibration position error introduces the additional component $-\mathbf{R}^T\mathbf{P}^{-1}\mathbf{R}$ in the matrix to be inverted. Applying the matrix inversion Lemma [22] to $((\mathbf{Z} - \mathbf{Y}^T\mathbf{X}^{-1}\mathbf{Y}) - \mathbf{R}^T\mathbf{P}^{-1}\mathbf{R})^{-1}$, substituting back into (10) and using $\text{CRLB}(\mathbf{u}^o)_{c^o}$ from (11) yield

$$\text{CRLB}(\mathbf{u}^o)_c - \text{CRLB}(\mathbf{u}^o)_{c^o} = \mathbf{X}^{-1}\mathbf{Y}\boldsymbol{\Upsilon}\mathbf{Y}^T\mathbf{X}^{-1} \tag{12}$$

where $\boldsymbol{\Upsilon} = \mathbf{B}^{-1}\mathbf{R}^T(\mathbf{P} - \mathbf{R}\mathbf{B}^{-1}\mathbf{R}^T)^{-1}\mathbf{R}\mathbf{B}^{-1}$ and $\mathbf{B} = (\mathbf{Z} - \mathbf{Y}^T\mathbf{X}^{-1}\mathbf{Y})$. The term on the right-hand side of (12) is the increase in the CRLB of a source location estimate due to the calibration position error. It is positive semidefinite because it has a symmetric structure, the matrix $\mathbf{R}$ defined in (8d) does not have full column rank and the matrix $(\mathbf{P} - \mathbf{R}\mathbf{B}^{-1}\mathbf{R}^T)$ is positive definite (see Appendix III). Hence, the best achievable localization accuracy with calibration position error will be worse than the one with accurate calibration emitter location information, as expected.

We shall come up with an alternative form of $\text{CRLB}(\mathbf{u}^o)_c$ to gain some physical insights. Define $\check{\mathbf{Z}}$ as $\check{\mathbf{Z}} = \mathbf{Z} - \mathbf{R}^T\mathbf{P}^{-1}\mathbf{R}$. Substituting the definitions of $\mathbf{Z}$, $\mathbf{R}$ and $\mathbf{P}$ from (8), applying the matrix inversion lemma [22] to the term $(\partial \tilde{\mathbf{r}}^o/\partial \mathbf{s}^o)^T\mathbf{Q}_c^{-1}(\partial \tilde{\mathbf{r}}^o/\partial \mathbf{s}^o) - \mathbf{R}^T\mathbf{P}^{-1}\mathbf{R}$ and simplifying, we can express $\check{\mathbf{Z}}$ as

$$\begin{aligned}\check{\mathbf{Z}} = \mathbf{Q}_\beta^{-1} + \left(\frac{\partial \mathbf{r}^o}{\partial \mathbf{s}^o}\right)^T \mathbf{Q}_\alpha^{-1}\left(\frac{\partial \mathbf{r}^o}{\partial \mathbf{s}^o}\right) \\ + \left(\frac{\partial \tilde{\mathbf{r}}^o}{\partial \mathbf{s}^o}\right)^T \left(\mathbf{Q}_c + \left(\frac{\partial \tilde{\mathbf{r}}^o}{\partial \mathbf{c}^o}\right)\mathbf{Q}_e\left(\frac{\partial \tilde{\mathbf{r}}^o}{\partial \mathbf{c}^o}\right)^T\right)^{-1}\left(\frac{\partial \tilde{\mathbf{r}}^o}{\partial \mathbf{s}^o}\right).\end{aligned} \tag{13}$$

Using the definition of $\check{\mathbf{Z}}$ in (10) gives an alternative expression of $\text{CRLB}(\mathbf{u}^o)_c$,

$$\text{CRLB}(\mathbf{u}^o)_c = \mathbf{X}^{-1} + \mathbf{X}^{-1}\mathbf{Y}(\check{\mathbf{Z}} - \mathbf{Y}^T\mathbf{X}^{-1}\mathbf{Y})^{-1}\mathbf{Y}^T\mathbf{X}^{-1}. \tag{14}$$

(14) has the same form as $\mathrm{CRLB}(\mathbf{u}^o)_{c^o}$ shown in (11), except that $\mathbf{Z}$ is replaced by $\check{\mathbf{Z}}$. From (8c) and (13), the difference between $\mathbf{Z}$ and $\check{\mathbf{Z}}$ lies in their third summands. The presence of calibration position error introduces an increment of $(\partial\tilde{\mathbf{r}}^o/\partial\mathbf{c}^o)\mathbf{Q}_e(\partial\tilde{\mathbf{r}}^o/\partial\mathbf{c}^o)^T$ into the matrix to be inverted. In other words, $\mathrm{CRLB}(\mathbf{u}^o)_c$ can be considered as the CRLB of an equivalent localization problem where the accurate calibration emitter position is available but the calibration measurements are degraded to have an increased covariance matrix of $\mathbf{Q}_c + (\partial\tilde{\mathbf{r}}^o/\partial\mathbf{c}^o)\mathbf{Q}_e(\partial\tilde{\mathbf{r}}^o/\partial\mathbf{c}^o)^T$. This observation leads to the interesting interpretation that the calibration position error affects the source localization accuracy through decreasing the quality of the calibration TDOA measurements.

We next examine the sensitivity of the CRLB of unknown source location in (14) to the calibration position error. For the special case when $\mathbf{Q}_e = \sigma_e^2\mathbf{I}$, where σ_e^2 is the calibration position noise power, it can be shown by applying (9c) that the $(i-1,k-1)$th element, $i,k = 2,3,\ldots,M$, of the matrix $(\partial\tilde{\mathbf{r}}^o/\partial\mathbf{c}^o)\mathbf{Q}_e(\partial\tilde{\mathbf{r}}^o/\partial\mathbf{c}^o)^T$ in (13) is $2\sigma_e^2(1-\cos\theta_{i1})$ if $i=k$ or $\sigma_e^2[(1-\cos\theta_{i1})(1-\cos\theta_{k1})+\sin\theta_{i1}\sin\theta_{k1}]$ if $i \neq k$. The angle θ_{i1} is the angle between the two vectors $\mathbf{c}^o - \mathbf{s}_1^o$ and $\mathbf{c}^o - \mathbf{s}_i^o$ counting from the former to the latter. By the law of cosines, its absolute value is $|\theta_{i1}| = |\arccos[(\tilde{r}_{i,1}^{o2} + \tilde{r}_{1,1}^{o2} - \|\mathbf{s}_i^o - \mathbf{s}_1^o\|^2)/(2\tilde{r}_{i,1}^o\tilde{r}_{1,1}^o)]|$, where $\tilde{r}_{i,1}^o = \|\mathbf{c}^o - \mathbf{s}_i^o\|$ is defined in (5) and $\mathbf{c}^o = \mathbf{c}_1^o$. When the calibration emitter $\mathbf{c}^o$ is far away from the sensor array, $|\theta_{i1}|$ would approach zero because in this case, $\tilde{r}_{i,1}^{o2} + \tilde{r}_{1,1}^{o2} \gg \|\mathbf{s}_i^o - \mathbf{s}_1^o\|^2$ and $\tilde{r}_{i,1}^o \simeq \tilde{r}_{1,1}^o$. As a result, the term that governs the increase in CRLB due to the calibration position error, $(\partial\tilde{\mathbf{r}}^o/\partial\mathbf{c}^o)\mathbf{Q}_e(\partial\tilde{\mathbf{r}}^o/\partial\mathbf{c}^o)^T$, would become close to a zero matrix. Hence, the CRLB of the unknown source position is less affected by the calibration position error when the calibration emitter is distant from the sensor array. Alternatively, it is more sensitive to the calibration position error if the calibration emitter is closer to the sensor array. For the general case where $\mathbf{Q}_e$ takes other form, similar observations can be obtained by noting that each row of $(\partial\tilde{\mathbf{r}}^o/\partial\mathbf{c}^o)$ is the difference of two unit vectors and the difference would become smaller as the calibration emitter moves farther away from the sensor array.

B. Improvement From Using a Calibration Emitter With Position Error

The CRLB without using a calibration emitter, denoted by $\mathrm{CRLB}(\mathbf{u}^o)_o$, is given in (12) of [17]. It has the same functional form as $\mathrm{CRLB}(\mathbf{u}^o)_c$ in (14), except that $\check{\mathbf{Z}}$ is replaced by $\hat{\mathbf{Z}} = \mathbf{Q}_\beta^{-1} + (\partial\mathbf{r}^o/\partial\mathbf{s}^o)^T\mathbf{Q}_\alpha^{-1}(\partial\mathbf{r}^o/\partial\mathbf{s}^o)$. From the definition of $\check{\mathbf{Z}}$ in (13), we note that the deployment of a calibration emitter introduces the additional term $(\partial\tilde{\mathbf{r}}^o/\partial\mathbf{s}^o)^T(\mathbf{Q}_c + (\partial\tilde{\mathbf{r}}^o/\partial\mathbf{c}^o)\mathbf{Q}_e(\partial\tilde{\mathbf{r}}^o/\partial\mathbf{c}^o)^T)^{-1}(\partial\tilde{\mathbf{r}}^o/\partial\mathbf{s}^o)$. Expressing $\check{\mathbf{Z}}$ in (13) in terms of $\hat{\mathbf{Z}}$, applying the matrix inversion Lemma [22] to the component $(\check{\mathbf{Z}} - \mathbf{Y}^T\mathbf{X}^{-1}\mathbf{Y})^{-1}$ in (14) and using the definition of $\mathrm{CRLB}(\mathbf{u}^o)_o$, it can be verified that $\mathrm{CRLB}(\mathbf{u}^o)_o - \mathrm{CRLB}(\mathbf{u}^o)_c$ is positive semidefinite. Hence, using a calibration emitter, although its position is not known exactly, remains to provide potential improvement in the source localization accuracy.

In the extreme case where the calibration emitter location is completely unknown, i.e., the covariance matrix of the calibration position error tends to infinity, it turns out that the difference $\mathrm{CRLB}(\mathbf{u}^o)_o - \mathrm{CRLB}(\mathbf{u}^o)_c$ remains positive semidefinite and non-zero. In other words, even if we have no knowledge about the calibration emitter location, the utilization of calibration TDOA measurements is still able to improve the source localization accuracy. This result has also been reported from previous studies [19], [20], [23], [24] on sensor network localization where signals of opportunity were used to improve performance.

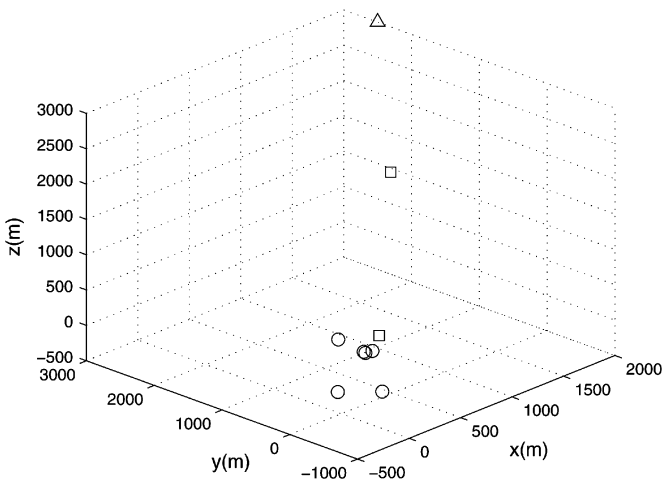

Fig. 2. Localization geometry for simulation. The open triangle is the unknown source location. The open circles represent the true sensor positions. The open squares denote the true possible calibration emitter positions.

TABLE I
TRUE POSITIONS (IN METERS) OF SENSORS

sensor no. i	$x_{s,i}^o$	$y_{s,i}^o$	$z_{s,i}^o$	sensor no. i	$x_{s,i}^o$	$y_{s,i}^o$	$z_{s,i}^o$
1	300	100	150	4	350	200	100
2	400	150	100	5	-100	-100	-100
3	300	500	200	6	200	-300	-200

C. Numerical Examples

To illustrate the CRLB results presented above, we generate some numerical values using the localization geometry depicted in Fig. 2. There are six sensors in total and their true positions are summarized in Table I. The distant unknown source $\mathbf{u}^o$ is positioned at $[2000, 2500, 3000]^T$ m. The calibration emitter $\mathbf{c}^o$ can either be at the position $[1500, 1550, 1500]^T$ m that is farther away from the sensor array or at $[450, 125, 300]^T$ m that is closer to the sensor array. The covariance matrices of the RDOA measurements are $\mathbf{Q}_\alpha = \mathbf{Q}_c = \sigma_r^2\mathbf{J}$, where $\sigma_r^2 = 10^{-3}$ and $\mathbf{J}$ is a square symmetric matrix whose diagonal elements are 1 and all other elements are 0.5. The setting for $\mathbf{Q}_\alpha$ and $\mathbf{Q}_c$ comes from the RDOA estimation process [16]. The covariance matrix of the sensor position error is chosen as $\mathbf{Q}_\beta = \sigma_s^2\mathbf{I}$ and that of the calibration position error is set to be $\mathbf{Q}_e = \sigma_e^2\mathbf{I}$ for simplicity. These settings for the noise covariance matrices are used for all the numerical examples and simulations in this paper. Nevertheless, all the analytical results and localization algorithms presented in this paper are still valid for any forms of noise covariance matrices.

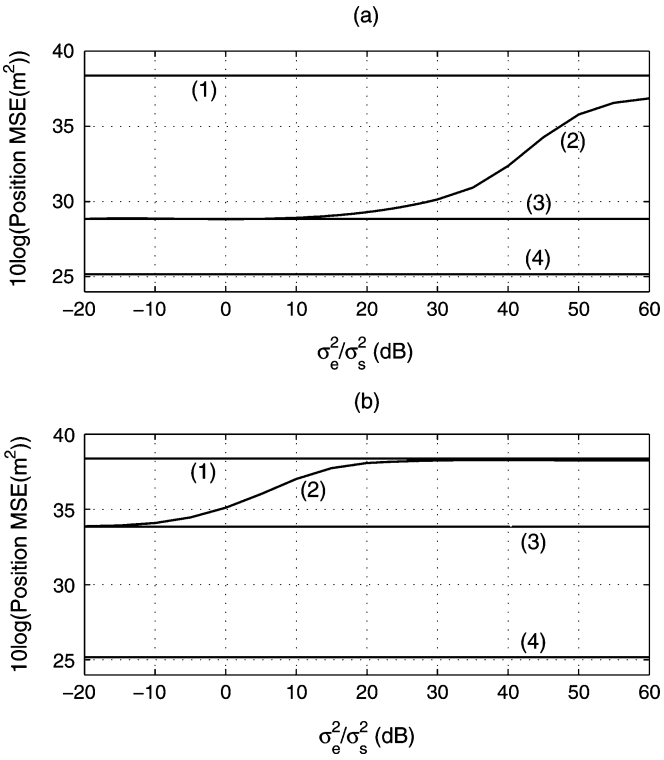

Fig. 3. Comparison of the CRLBs of $\mathbf{u}^o$ as a function of normalized calibration position noise power σ_e^2/σ_s^2 when a calibration emitter is present. (a) Calibration emitter farther away from the sensor array. (b) Calibration emitter closer to the sensor array. (1) $\mathrm{tr}(\mathrm{CRLB}(\mathbf{u}^o)_o)$ from (12) in [17], (2) $\mathrm{tr}(\mathrm{CRLB}(\mathbf{u}^o)_c)$ from (10), (3) $\mathrm{tr}(\mathrm{CRLB}(\mathbf{u}^o)_{c^o})$ from (11), (4) $\mathrm{tr}(\mathrm{CRLB}(\mathbf{u}^o))$.

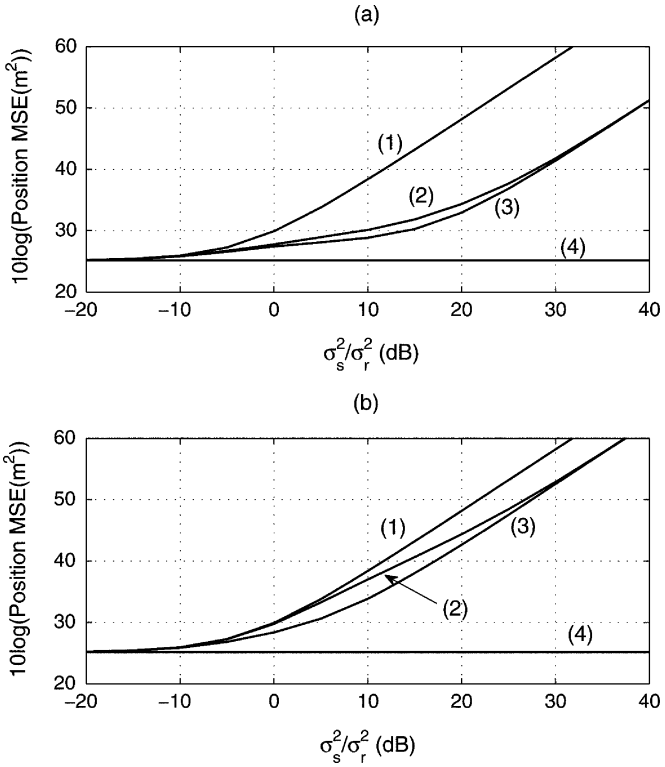

Fig. 4. Comparison of the CRLBs of $\mathbf{u}^o$ as a function of normalized sensor position noise power σ_s^2/σ_r^2 when a calibration emitter is present. (a) Calibration emitter farther away from the sensor array. (b) Calibration emitter closer to the sensor array. (1) $\mathrm{tr}(\mathrm{CRLB}(\mathbf{u}^o)_o)$ from (12) in [17], (2) $\mathrm{tr}(\mathrm{CRLB}(\mathbf{u}^o)_c)$ from (10), (3) $\mathrm{tr}(\mathrm{CRLB}(\mathbf{u}^o)_{c^o})$ from (11), (4) $\mathrm{tr}(\mathrm{CRLB}(\mathbf{u}^o))$.

We examine, in Fig. 3, the effect of calibration position error on the source localization accuracy by varying the calibration position noise power σ_e^2. σ_s^2 is fixed at -20 in log scale $(10\log_{10}(\sigma_s^2))$ and the trace of $\mathrm{CRLB}(\mathbf{u}^o)_c$ from (10) (curve (2)) is plotted as a function of σ_e^2/σ_s^2. The traces of $\mathrm{CRLB}(\mathbf{u}^o)_o$ (curve (1)), $\mathrm{CRLB}(\mathbf{u}^o)_{c^o}$ (curve (3)) and $\mathrm{CRLB}(\mathbf{u}^o)$ (curve (4)) are also shown for comparison. Fig. 3(a) gives the results when $\mathbf{c}^o = [1500, 1550, 1500]^T$ m. It is evident that the lower bound of source localization error with calibration position uncertainty (curve (2)) is always larger than the one without (curve (3)) and this is consistent with the analytical result in (12). On the other hand, when σ_e^2/σ_s^2 becomes sufficiently large, i.e., the given calibration emitter position becomes highly unreliable, the bound approaches 37 in log scale, the value of the bound when the calibration emitter location is completely unknown. Interestingly, even with no knowledge of the calibration emitter position, using the calibration TDOAs remains to provide an improvement, in this simulation, of 1.38 dB over the case without using the calibration source (curve (1)).

The CRLB results for $\mathbf{c}^o = [450, 125, 300]^T$ m are shown in Fig. 3(b). The observations are similar to those from Fig. 3(a). The lower bound with calibration position error (curve (2)) converges to 38.27 in log scale, which is 0.11 dB lower than the case without using the calibration emitter (curve (1)). Besides, it starts deviating from the one without calibration position error (curve (3)) when $\sigma_e^2/\sigma_s^2 \geq -10$ dB, which is 20 dB earlier compared to the case when the calibration emitter is far from the sensor array. This observation confirms the analysis at the end of Section III-A that the CRLB of the unknown source location is more sensitive to the calibration position error, when the calibration emitter is closer to the sensor array.

We next examine, in Fig. 4, the effect of varying the amount of sensor position noise power on the localization performance. In this simulation, the calibration position noise power σ_e^2 is set to be 10 in log scale for Fig. 4(a) and -10 in log scale for Fig. 4(b). The traces of $\mathrm{CRLB}(\mathbf{u}^o)_c$ (curve (2)), $\mathrm{CRLB}(\mathbf{u}^o)_{c^o}$ (curve (3)), $\mathrm{CRLB}(\mathbf{u}^o)_o$ (curve (1)) and $\mathrm{CRLB}(\mathbf{u}^o)$ (curve (4)) are depicted as a function of σ_s^2/σ_r^2. When the calibration emitter farther away from the sensor array is used, Fig. 4(a) shows that the calibration position error degrades the source localization accuracy only when the sensor position noise power is comparable to or moderately bigger than the RDOA measurement noise power (0 dB $\leq \sigma_s^2/\sigma_r^2 \leq 30$ dB). When $\sigma_s^2/\sigma_r^2 \geq 35$ dB, the difference between the bounds with and without calibration position error (curve (2) and curve (3)) would become very small. This is because in this case, the calibration position is relatively accurate compared to the sensor positions. Fig. 4(b) plots the CRLB results when the calibration emitter is closer to the sensor array and it exhibits similar trends as in Fig. 4(a). Here, the calibration position error causes considerable degradation in the source localization accuracy over a wider range of sensor position noise power (-10 dB $\leq \sigma_s^2/\sigma_r^2 \leq 30$ dB). This can be attributed to the analysis result in Section III-A that the localization accuracy is degraded more by the calibration position error when the distance between the calibration emitter and the sensor array is small.

Another important observation from the curves (3) and (4) in Fig. 4 is that the presence of sensor position error, even a small amount, could significantly reduce the localization accuracy. Hence, if we have the freedom to decide which are the receiving sensors and which are the calibration emitters from a number of sensors equipped with transceivers, one criterion could be to select those with smaller position errors as receiving sensors while allocating others as calibration emitters. The optimal grouping of receiving and calibration sensors depends on other factors as well, such as the localization geometry. Finding the optimum grouping scheme is an interesting problem to explore in the subsequent research.

IV. Analysis When Ignoring Calibration Position Error

In this section, we shall investigate the effect of neglecting calibration position error on the source localization accuracy when using a single calibration emitter. The MSE matrix of a source location estimate is related to the calibration position error in a non-linear manner. This section performs a first-order analysis to simplify the development and gain insights. The derived results are therefore valid only when the calibration position error is not large. Under first-order approximation, the source location estimate becomes unbiased and the MSE matrix is equal to its covariance matrix. We shall compare the obtained covariance matrix of the source location estimate with the CRLB from the last section to quantify the performance degradation due to the ignorance of the calibration position error. Simulations are provided at the end of the section to confirm the theoretical development.

Suppose we would like to jointly estimate the source location $\mathbf{u}^o$ and the true sensor position vector $\mathbf{s}^o$ using the RDOA measurements from the unknown source and the calibration emitter. The available calibration emitter position $\mathbf{c}$ is assumed to be exact, although it has error. Denote the corresponding estimates of $\mathbf{u}^o$ and $\mathbf{s}^o$ as $\check{\mathbf{u}}$ and $\check{\mathbf{s}}$ and collect them as $\check{\boldsymbol{\theta}} = [\check{\mathbf{u}}^T, \check{\mathbf{s}}^T]^T$. The pseudo ML cost function when pretending that the calibration position error is absent is

$$(\mathbf{m} - \mathbf{g}(\check{\boldsymbol{\theta}}))^T \mathbf{W}^{-1} (\mathbf{m} - \mathbf{g}(\check{\boldsymbol{\theta}})) \tag{15}$$

where $\mathbf{m} = [\mathbf{r}^T, \tilde{\mathbf{r}}^T, \mathbf{s}^T]^T = \mathbf{m}^o + \Delta\mathbf{m}$ is the composite measurement vector, $\mathbf{m}^o = [\mathbf{r}^{oT}, \tilde{\mathbf{r}}^{oT}, \mathbf{s}^{oT}]^T$ is the ideal measurement vector without noise, and $\Delta\mathbf{m} = [\mathbf{n}^T, \tilde{\mathbf{n}}^T, \boldsymbol{\Psi}^T]^T$ is the measurement noise vector. $\mathbf{g}(\check{\boldsymbol{\theta}})$ is the constructed measurement vector using the estimate $\check{\boldsymbol{\theta}}$ and the calibration emitter position $\mathbf{c}$. It is equal to $\mathbf{g}(\check{\boldsymbol{\theta}}) = [\mathbf{r}(\check{\boldsymbol{\theta}})^T, \tilde{\mathbf{r}}(\check{\boldsymbol{\theta}})^T, \check{\mathbf{s}}^T]^T$, where $\mathbf{r}(\check{\boldsymbol{\theta}}) = [r_{21}(\check{\boldsymbol{\theta}}), r_{31}(\check{\boldsymbol{\theta}}), \ldots, r_{M1}(\check{\boldsymbol{\theta}})]^T$, $\tilde{\mathbf{r}}(\check{\boldsymbol{\theta}}) = [\tilde{r}_{21}(\check{\boldsymbol{\theta}}), \tilde{r}_{31}(\check{\boldsymbol{\theta}}), \ldots, \tilde{r}_{M1}(\check{\boldsymbol{\theta}})]^T$,

$$r_{k1}(\check{\boldsymbol{\theta}}) = \|\check{\mathbf{u}} - \check{\mathbf{s}}_k\| - \|\check{\mathbf{u}} - \check{\mathbf{s}}_1\|, \quad k = 2, 3, \ldots, M \tag{16a}$$

$$\tilde{r}_{k1}(\check{\boldsymbol{\theta}}) = \|\mathbf{c} - \check{\mathbf{s}}_k\| - \|\mathbf{c} - \check{\mathbf{s}}_1\|, \quad k = 2, 3, \ldots, M. \tag{16b}$$

$\mathbf{W}$ is the covariance matrix of $\mathbf{m}$, i.e.,

$$\mathbf{W} = \mathrm{cov}(\Delta\mathbf{m}) = \mathrm{diag}[\mathbf{Q}_\alpha, \mathbf{Q}_c, \mathbf{Q}_\beta]. \tag{17}$$

$\mathbf{g}(\check{\boldsymbol{\theta}})$ is a non-linear function of $\check{\boldsymbol{\theta}}$. If we linearize $\mathbf{g}(\check{\boldsymbol{\theta}})$ around $\check{\boldsymbol{\theta}} = \boldsymbol{\theta}^o$, where $\boldsymbol{\theta}^o = [\mathbf{u}^{oT}, \mathbf{s}^{oT}]^T$ is the true solution, the first-order approximation is

$$\mathbf{g}(\check{\boldsymbol{\theta}}) \simeq \mathbf{g}(\boldsymbol{\theta}^o) + \mathbf{G}(\boldsymbol{\theta}^o)(\check{\boldsymbol{\theta}} - \boldsymbol{\theta}^o) \tag{18}$$

where $\mathbf{g}(\boldsymbol{\theta}^o) = [\mathbf{r}^{oT}, \tilde{\mathbf{r}}(\boldsymbol{\theta}^o)^T, \mathbf{s}^{oT}]^T$ and $\mathbf{G}(\boldsymbol{\theta}^o)$ is the Jacobian matrix defined as

$$\mathbf{G}(\boldsymbol{\theta}^o) = \begin{bmatrix} \left(\frac{\partial \mathbf{r}(\check{\boldsymbol{\theta}})}{\partial \check{\mathbf{u}}}\right)\Big|_{\boldsymbol{\theta}^o} & \left(\frac{\partial \mathbf{r}(\check{\boldsymbol{\theta}})}{\partial \check{\mathbf{s}}}\right)\Big|_{\boldsymbol{\theta}^o} \\ \mathbf{O}_{(M-1)\times 3} & \left(\frac{\partial \tilde{\mathbf{r}}(\check{\boldsymbol{\theta}})}{\partial \check{\mathbf{s}}}\right)\Big|_{\boldsymbol{\theta}^o} \\ \mathbf{O}_{3M\times 3} & \mathbf{I}_{3M\times 3M} \end{bmatrix}. \tag{19}$$

The first-order approximation (18) is valid when the power of the measurement noise $\Delta\mathbf{m}$ is small so that $\check{\boldsymbol{\theta}}$ is not too much deviated from $\boldsymbol{\theta}^o$. Comparing (16a) and (4), we notice immediately that $(\partial \mathbf{r}(\check{\boldsymbol{\theta}})/\partial \check{\mathbf{u}})|_{\boldsymbol{\theta}^o}$ and $(\partial \mathbf{r}(\check{\boldsymbol{\theta}})/\partial \check{\mathbf{s}})|_{\boldsymbol{\theta}^o}$ are equal to $(\partial \mathbf{r}^o/\partial \mathbf{u}^o)$ and $(\partial \mathbf{r}^o/\partial \mathbf{s}^o)$ defined through (9a) and (9b). Furthermore, it can be seen from (16b) and (5) that $(\partial \tilde{\mathbf{r}}(\check{\boldsymbol{\theta}})/\partial \check{\mathbf{s}})|_{\boldsymbol{\theta}^o}$ has the same functional form as $(\partial \tilde{\mathbf{r}}^o/\partial \mathbf{s}^o)$ defined through (9d), except that the true calibration emitter position $\mathbf{c}^o$ is replaced by its noisy version $\mathbf{c}$. Substituting (18) into (15) and solving the minimization problem give

$$\check{\boldsymbol{\theta}} = \boldsymbol{\theta}^o + (\mathbf{G}(\boldsymbol{\theta}^o)^T \mathbf{W}^{-1} \mathbf{G}(\boldsymbol{\theta}^o))^{-1} \mathbf{G}(\boldsymbol{\theta}^o)^T \mathbf{W}^{-1} (\mathbf{m} - \mathbf{g}(\boldsymbol{\theta}^o)). \tag{20}$$

Subtracting the true solution $\boldsymbol{\theta}^o$ from both sides of (20) yields the estimation error

$$\boldsymbol{\epsilon} = \check{\boldsymbol{\theta}} - \boldsymbol{\theta}^o = (\mathbf{G}(\boldsymbol{\theta}^o)^T \mathbf{W}^{-1} \mathbf{G}(\boldsymbol{\theta}^o))^{-1} \times \mathbf{G}(\boldsymbol{\theta}^o)^T \mathbf{W}^{-1} (\mathbf{m} - \mathbf{g}(\boldsymbol{\theta}^o)) \tag{21}$$

where the first three elements of $\boldsymbol{\epsilon}$ are the components of the source localization error.

The estimation error $\boldsymbol{\epsilon}$ is non-linear with respect to the calibration position error, because the noisy calibration emitter position $\mathbf{c}$ appears in both $\mathbf{G}(\boldsymbol{\theta}^o)$ and $\mathbf{g}(\boldsymbol{\theta}^o)$. As a result, it is very difficult to derive the covariance matrix of $\boldsymbol{\epsilon}$ through direct evaluation of $E[\boldsymbol{\epsilon}\boldsymbol{\epsilon}^T]$ from (21). Assuming the calibration position error is small so that the difference between $(\partial \tilde{\mathbf{r}}(\check{\boldsymbol{\theta}})/\partial \check{\mathbf{s}})|_{\boldsymbol{\theta}^o}$ and $(\partial \tilde{\mathbf{r}}^o/\partial \mathbf{s}^o)$ is negligible, $\mathbf{G}(\boldsymbol{\theta}^o)$ can be approximated by $\bar{\mathbf{G}}$ as

$$\bar{\mathbf{G}} = \begin{bmatrix} \left(\frac{\partial \mathbf{r}^o}{\partial \mathbf{u}^o}\right)_{(M-1)\times 3} & \left(\frac{\partial \mathbf{r}^o}{\partial \mathbf{s}^o}\right)_{(M-1)\times 3M} \\ \mathbf{O}_{(M-1)\times 3} & \left(\frac{\partial \tilde{\mathbf{r}}^o}{\partial \mathbf{s}^o}\right)_{(M-1)\times 3M} \\ \mathbf{O}_{3M\times 3} & \mathbf{I}_{3M\times 3M} \end{bmatrix}. \tag{22}$$

Correspondingly, the estimation error $\boldsymbol{\epsilon}$ would become

$$\boldsymbol{\epsilon} = (\bar{\mathbf{G}}^T \mathbf{W}^{-1} \bar{\mathbf{G}})^{-1} \bar{\mathbf{G}}^T \mathbf{W}^{-1} (\mathbf{m} - \mathbf{g}(\boldsymbol{\theta}^o)). \tag{23}$$

We proceed to simplify $(\mathbf{m} - \mathbf{g}(\boldsymbol{\theta}^o))$. Linearizing $\tilde{\mathbf{r}}(\boldsymbol{\theta}^o)$ around $\mathbf{c}^o$ up to the first-order term yields, using (16b),

$$\tilde{\mathbf{r}}(\boldsymbol{\theta}^o) \simeq \tilde{\mathbf{r}}(\boldsymbol{\theta}^o)|_{\mathbf{c}^o} + \mathbf{H} \cdot \mathbf{e} \tag{24}$$

where $\mathbf{H} = (\partial\tilde{\mathbf{r}}^o/\partial\mathbf{c}^o)$ and $\mathbf{e} = \mathbf{c} - \mathbf{c}^o$. Note that $\tilde{\mathbf{r}}(\boldsymbol{\theta}^o)|_{\mathbf{c}^o}$ is in fact identical to $\tilde{\mathbf{r}}^o$ defined below (5). Substituting $\mathbf{m} = \mathbf{m}^o + \Delta\mathbf{m}$ and using (24), we have

$$\mathbf{m} - \mathbf{g}(\boldsymbol{\theta}^o) = \Delta\mathbf{m} - \left[\mathbf{0}^T_{(M-1)\times 1},\ (\mathbf{H}\cdot\mathbf{e})^T, \mathbf{0}^T_{3M\times 1}\right]^T. \quad (25)$$

The covariance matrix of (25) is, since $\Delta\mathbf{m}$ and $\mathbf{e}$ are uncorrelated

$$\mathrm{cov}(\mathbf{m} - \mathbf{g}(\boldsymbol{\theta}^o)) = \mathbf{W} + \mathbf{M} \quad (26)$$

where $\mathbf{W}$ is given in (17) and $\mathbf{M}$ is defined as

$$\mathbf{M} = \mathrm{diag}\left[\mathbf{O}_{(M-1)\times(M-1)}, \mathbf{H}\mathbf{Q}_e\mathbf{H}^T, \mathbf{O}_{3M\times 3M}\right]. \quad (27)$$

Putting (25) into (23) and taking expectation show that $\boldsymbol{\epsilon}$ is zero mean because $\Delta\mathbf{m}$ and $\mathbf{e}$ are zero mean. Hence, $\check{\boldsymbol{\theta}}$ is unbiased under first-order approximation. Multiplying (23) with its transpose, taking expectation and simplifying yield the covariance matrix of $\check{\boldsymbol{\theta}}$

$$\mathrm{cov}(\check{\boldsymbol{\theta}}) = (\bar{\mathbf{G}}^T\mathbf{W}^{-1}\bar{\mathbf{G}})^{-1} + (\bar{\mathbf{G}}^T\mathbf{W}^{-1}\bar{\mathbf{G}})^{-1}\bar{\mathbf{G}}^T\mathbf{W}^{-1} \times\mathbf{M}\mathbf{W}^{-1}\bar{\mathbf{G}}(\bar{\mathbf{G}}^T\mathbf{W}^{-1}\bar{\mathbf{G}})^{-1}. \quad (28)$$

Note that the covariance matrix of the calibration position error $\mathbf{Q}_e$ only appears in $\mathbf{M}$, as shown in (27). The contribution of the calibration position noise to the estimation accuracy of $\check{\boldsymbol{\theta}}$ is governed by the matrix $\mathbf{H}$ defined under (24), whose $(i-1)$th row, $i = 2, 3, \ldots, M$, is given in (9c). By following the same argument at the end of Section III-A that is used to analyze the sensitivity of the source location CRLB to the calibration position error, we obtain a similar conclusion that the estimation accuracy of $\check{\boldsymbol{\theta}}$ is more sensitive to the position error of the calibration emitter when it is located closer to the sensor array.

The covariance matrix of the source location estimate $\check{\mathbf{u}}$ is the upper left three-by-three block of $\mathrm{cov}(\check{\boldsymbol{\theta}})$. As shown in Appendix IV, it is equal to

$$\mathrm{cov}(\check{\mathbf{u}}) = \mathrm{CRLB}(\mathbf{u}^o)_{c^o} + \mathbf{X}^{-1}\mathbf{Y}\mathbf{B}^{-1}\mathbf{R}^T\mathbf{Q}_e\mathbf{R}\mathbf{B}^{-1}\mathbf{Y}^T\mathbf{X}^{-1} \quad (29)$$

where $\mathrm{CRLB}(\mathbf{u}^o)_{c^o}$ is given in (11), $\mathbf{X}$, $\mathbf{Y}$, and $\mathbf{R}$ are given in (8a), (8b) and (8d), respectively, and $\mathbf{B}$ is defined under (12). When both the RDOA noise and the calibration position error are not large, the covariance matrix of $\check{\mathbf{u}}$ in (29) is applicable to any location estimator that can achieve the CRLB accuracy in the absence of calibration position error.

We next compare $\mathrm{cov}(\check{\mathbf{u}})$ with $\mathrm{CRLB}(\mathbf{u}^o)_c$, the best achievable localization accuracy in the presence of position errors in both the sensors and the calibration emitter. Subtracting (12) from (29), using the definition of $\boldsymbol{\Upsilon}$ under (12) and simplifying yield

$$\mathrm{cov}(\check{\mathbf{u}}) - \mathrm{CRLB}(\mathbf{u}^o)_c = \mathbf{X}^{-1}\mathbf{Y}\mathbf{B}^{-1}\mathbf{R}^T \times(\mathbf{Q}_e - (\mathbf{P} - \mathbf{R}\mathbf{B}^{-1}\mathbf{R}^T)^{-1})\mathbf{R}\mathbf{B}^{-1}\mathbf{Y}^T\mathbf{X}^{-1} \quad (30)$$

where $\mathbf{P}$ is defined in (8e). The term on the right-hand side of (30) is the performance degradation with respect to the CRLB resulted from ignoring the calibration position error. From (62) and the discussion following (62) in Appendix III, we have that $(\mathbf{P} - \mathbf{R}\mathbf{B}^{-1}\mathbf{R}^T) - \mathbf{Q}_e^{-1}$ is positive definite. Hence, $\mathbf{Q}_e - (\mathbf{P} - \mathbf{R}\mathbf{B}^{-1}\mathbf{R}^T)^{-1}$ is also positive definite. Since $\mathbf{R}$ does not have full column rank, the entire matrix on the right of (30) is positive semidefinite. In other words, if we do not take the calibration position error into consideration, the source position estimate will not reach the CRLB accuracy. Indeed, the difference between $\mathrm{cov}(\check{\mathbf{u}})$ and the CRLB can be very significant even when the calibration position error is not large, as illustrated in the example below.

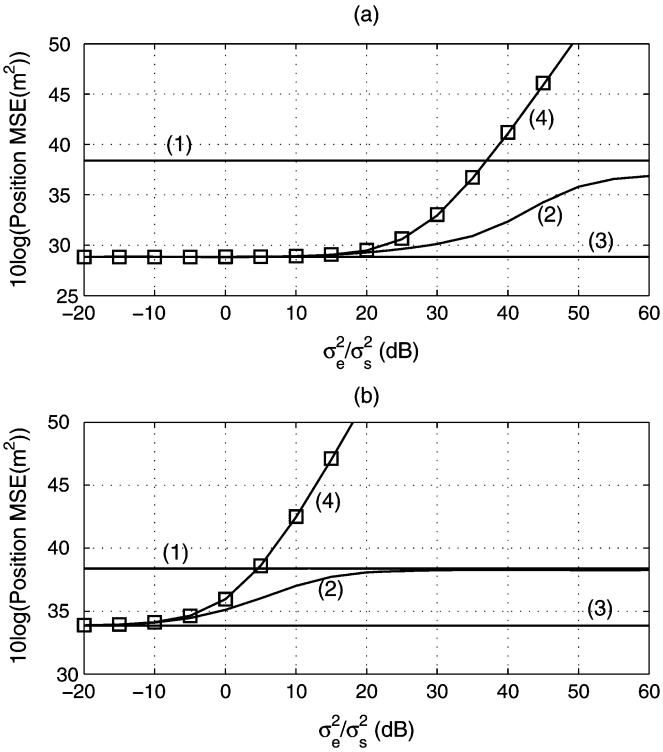

Fig. 5. Comparison of the CRLBs of $\mathbf{u}^o$ and the localization MSE when assuming no calibration position error in the single calibration emitter scenario. (a) Calibration emitter farther away from the sensor array. (b) Calibration emitter closer to the sensor array. (1) $\mathrm{tr}(\mathrm{CRLB}(\mathbf{u}^o)_o)$ from (12) in [17], (2) $\mathrm{tr}(\mathrm{CRLB}(\mathbf{u}^o)_c)$ from (10), (3) $\mathrm{tr}(\mathrm{CRLB}(\mathbf{u}^o)_{c^o})$ from (11), (4) $\mathrm{tr}(\mathrm{cov}(\check{\mathbf{u}}))$ from (29), simulation MSE from the solution in [18]: square symbol.

We plot in Fig. 5 the trace of $\mathrm{cov}(\check{\mathbf{u}})$, the MSE of the source location estimate when ignoring the calibration position error, as a function of the calibration position noise power over the sensor position noise power σ_e^2/σ_s^2, where σ_s^2 is set to -20 in log scale. The localization geometry is the same as that in Fig. 2. The RDOA noise settings are the same as in Section III-C. The upper plot is for $\mathbf{c}^o = [1500, 1550, 1500]^T$ m that is far from the sensor array and the lower is for $\mathbf{c}^o = [450, 125, 300]^T$ m that is close to the sensor array. The algorithm proposed in [18] was used to estimate the unknown source position and the corresponding localization MSE is obtained by an average of 10^4 ensemble runs. In each ensemble run, the noisy RDOAs and the erroneous sensor and calibration emitter positions are created by adding newly generated noises to the true values. The MSEs from simulation are shown in square symbol and the solid line (4) is from the formula (29). The simulation results match the theoretical values quite well. When contrasting with the best achievable accuracy $\mathrm{tr}(\mathrm{CRLB}(\mathbf{u}^o)_c)$ (curve (2)), $\mathrm{tr}(\mathrm{cov}(\check{\mathbf{u}}))$

(curve (4)) is always greater, which is consistent with the analytical result in (30). Moreover, comparing Fig. 5(a) and (b) reveals that $\mathrm{tr}(\mathrm{cov}(\check{\mathbf{u}}))$ starts to deviate from $\mathrm{tr}(\mathrm{CRLB}(\mathbf{u}^o)_c)$ at a smaller value of σ_e^2/σ_s^2 when the calibration emitter is closer to the sensor array. This observation is expected from the analysis under (28) that the calibration position noise affects the source location estimate $\check{\mathbf{u}}$ more if the calibration emitter is closer to the sensor array. Finally, as σ_e^2/σ_s^2 increases, the difference between $\mathrm{tr}(\mathrm{cov}(\check{\mathbf{u}}))$ and $\mathrm{tr}(\mathrm{CRLB}(\mathbf{u}^o)_c)$ grows rapidly. After σ_e^2/σ_s^2 reaches a certain value (as low as 5 dB in Fig. 5(b)), the location MSE of $\check{\mathbf{u}}$ becomes even greater than the one without a calibration source. This observation can be inferred from (29) that the MSE of $\check{\mathbf{u}}$ is proportional to the covariance matrix of the calibration position error $\mathbf{Q}_e$, but the one without using the calibration emitter does not depend on it. Hence, in order to improve the accuracy by exploiting the calibration emitter, it is necessary to take the calibration position error into account when designing a source localization algorithm.

V. Closed-Form Localization Algorithm

This section extends the algebraic localization algorithm presented in [18] to estimate the unknown source position in the presence of sensor and calibration position errors. The proposed solution is closed-form and computationally attractive. Furthermore, the proposed solution will be shown analytically to reach the CRLB accuracy when certain conditions are met. The new method is developed next and the theoretical analysis on its localization performance will follow.

A. Algorithm

The proposed solution is composed of three stages. The first stage uses the calibration RDOA measurements to improve the sensor positions. The statistical knowledge of the calibration position error is explicitly exploited to guarantee that the updated sensor positions are statistically as good as, if not better than, the original ones. The remaining two stages utilize the improved sensor positions and the RDOA measurements from the unknown source to estimate its position. These two stages are the same as those in the solution developed in [18]. We shall present the first stage of the new algorithm in details. The computations of the second and third stages are summarized for the completeness of the proposed algorithm.

First Stage: Using the noisy sensor positions $\mathbf{s}_i$ and the erroneous calibration emitter position $\mathbf{c}$, we can generate a predicted version of the calibration RDOAs

$$\hat{r}_{i1,1} = \|\mathbf{c}-\mathbf{s}_i\| - \|\mathbf{c}-\mathbf{s}_1\|, \quad i = 2,3,\ldots,M. \tag{31}$$

Subtracting $\hat{r}_{i1,1}$ from $\tilde{r}_{i1,1}$ in (3b) yields the difference between the measured calibration RDOA and its prediction

$$\tilde{r}_{i1,1} - \hat{r}_{i1,1} = \tilde{r}^o_{i1,1} - \|\mathbf{c}-\mathbf{s}_i\| + \|\mathbf{c}-\mathbf{s}_1\| + \tilde{n}_{i1,1}, \quad i = 2,3,\ldots,M. \tag{32}$$

After substituting the definition of $\tilde{r}^o_{i1,1}$ in (5) and the error models (1) and (2), we arrive at

$$\tilde{r}_{i1,1} - \hat{r}_{i1,1} = (\|\mathbf{c}-\mathbf{e}-\mathbf{s}_i+\boldsymbol{\Psi}_i\| - \|\mathbf{c}-\mathbf{s}_i\|) - (\|\mathbf{c}-\mathbf{e}-\mathbf{s}_1+\boldsymbol{\Psi}_1\| - \|\mathbf{c}-\mathbf{s}_1\|) + \tilde{n}_{i1,1}. \tag{33}$$

(33) indicates that the value of $\tilde{r}_{i1,1} - \hat{r}_{i1,1}$ indeed contains information regarding the realizations of the random sensor position errors $\boldsymbol{\Psi}_i$. Our interest is to obtain an estimate of $\boldsymbol{\Psi}_i$ from $\tilde{r}_{i1,1} - \hat{r}_{i1,1}$ in order to improve the sensor positions. The above task is non-trivial, since we have to take the calibration position error $\mathbf{e}$ into account when estimating $\boldsymbol{\Psi}_i$. Furthermore, the estimation is complicated by the fact that the difference $\tilde{r}_{i1,1} - \hat{r}_{i1,1}$ is non-linearly related to both $\boldsymbol{\Psi}_i$ and $\mathbf{e}$, as shown in (33). To address these difficulties, we expand $\|\mathbf{c}-\mathbf{e}-\mathbf{s}_i+\boldsymbol{\Psi}_i\|$ up to the linear terms of $\boldsymbol{\Psi}_i$ and $\mathbf{e}$ as

$$\|\mathbf{c}-\mathbf{e}-\mathbf{s}_i+\boldsymbol{\Psi}_i\| \simeq \|\mathbf{c}-\mathbf{s}_i\| + \boldsymbol{\rho}^T_{\mathbf{c},\mathbf{s}_i}\boldsymbol{\Psi}_i - \boldsymbol{\rho}^T_{\mathbf{c},\mathbf{s}_i}\mathbf{e}. \tag{34}$$

Putting (34) back into (33) and simplifying yield

$$\tilde{r}_{i1,1} - \hat{r}_{i1,1} \simeq \boldsymbol{\rho}^T_{\mathbf{c},\mathbf{s}_i}\boldsymbol{\Psi}_i - \boldsymbol{\rho}^T_{\mathbf{c},\mathbf{s}_1}\boldsymbol{\Psi}_1 + \left(\boldsymbol{\rho}^T_{\mathbf{c},\mathbf{s}_1} - \boldsymbol{\rho}^T_{\mathbf{c},\mathbf{s}_i}\right)\cdot\mathbf{e} + \tilde{n}_{i1,1}. \tag{35}$$

Expressing (35) in matrix form, we have

$$\mathbf{h}_c = \mathbf{G}_c\boldsymbol{\Psi} + \mathbf{G}_e\cdot\mathbf{e} + \tilde{\mathbf{n}} \tag{36}$$

where $\mathbf{h}_c = [\tilde{r}_{21,1} - \hat{r}_{21,1}, \tilde{r}_{31,1} - \hat{r}_{31,1}, \ldots, \tilde{r}_{M1,1} - \hat{r}_{M1,1}]^T$ and $\tilde{\mathbf{n}}$ is the calibration RDOA noise vector. $\boldsymbol{\Psi}$ is the composite sensor position error vector defined below (1). $\mathbf{G}_c$ is an $(M-1)\times 3M$ matrix and $\mathbf{G}_e$ is an $(M-1)\times 3$ matrix. The $(i-1)$th rows of $\mathbf{G}_c$ and $\mathbf{G}_e$, $i = 2,3,\ldots,M$, are

$$\mathbf{G}_c[i-1,:] = \left[-\boldsymbol{\rho}^T_{\mathbf{c},\mathbf{s}_1}, \underbrace{\mathbf{0}^T}_{1\times 3(i-2)}, \boldsymbol{\rho}^T_{\mathbf{c},\mathbf{s}_i}, \underbrace{\mathbf{0}^T}_{1\times 3(M-i)}\right] \tag{37a}$$

$$\mathbf{G}_e[i-1,:] = \left[\boldsymbol{\rho}^T_{\mathbf{c},\mathbf{s}_1} - \boldsymbol{\rho}^T_{\mathbf{c},\mathbf{s}_i}\right]. \tag{37b}$$

We shall estimate $\boldsymbol{\Psi}$ based on the linear model (36). As specified in Section II, $\boldsymbol{\Psi}$ is a zero mean Gaussian random vector with covariance matrix $\mathbf{Q}_\beta$. The term $\mathbf{G}_e\cdot\mathbf{e}+\tilde{\mathbf{n}}$ follows a multivariate Gaussian distribution with mean $\mathbf{0}_{(M-1)\times 1}$ and covariance matrix $\mathbf{G}_e\mathbf{Q}_e\mathbf{G}_e^T+\mathbf{Q}_c$, because $\mathbf{e}$ and $\tilde{\mathbf{n}}$ are independent zero mean Gaussian random vectors with covariance matrices $\mathbf{Q}_e$ and $\mathbf{Q}_c$. Applying the Bayesian Gauss–Markov theorem [21], we obtain the linear minimum MSE (LMMSE) estimate of $\boldsymbol{\Psi}$ as

$$\hat{\boldsymbol{\Psi}} = \left(\mathbf{Q}_\beta^{-1} + \mathbf{G}_c^T\left(\mathbf{G}_e\mathbf{Q}_e\mathbf{G}_e^T+\mathbf{Q}_c\right)^{-1}\mathbf{G}_c\right)^{-1} \times\mathbf{G}_c^T\left(\mathbf{G}_e\mathbf{Q}_e\mathbf{G}_e^T+\mathbf{Q}_c\right)^{-1}\mathbf{h}_c. \tag{38}$$

The covariance matrix of $\hat{\boldsymbol{\Psi}}$ is

$$\mathrm{cov}(\boldsymbol{\Psi}-\hat{\boldsymbol{\Psi}}) = \left(\mathbf{Q}_\beta^{-1} + \mathbf{G}_c^T\left(\mathbf{G}_e\mathbf{Q}_e\mathbf{G}_e^T+\mathbf{Q}_c\right)^{-1}\mathbf{G}_c\right)^{-1}. \tag{39}$$

Subtracting $\hat{\boldsymbol{\Psi}}$ from the original sensor position vector $\mathbf{s}$ yields the improved sensor position vector $\hat{\mathbf{s}}$, that is,

$$\hat{\mathbf{s}} = \mathbf{s} - \hat{\boldsymbol{\Psi}}. \tag{40}$$

Note that since $\mathbf{s} = \mathbf{s}^o + \boldsymbol{\Psi}$, $\hat{\mathbf{s}}$ can be expressed as $\hat{\mathbf{s}} = \mathbf{s}^o + \boldsymbol{\Psi} - \hat{\boldsymbol{\Psi}}$. The covariance matrix of $\hat{\mathbf{s}}$ is identical to the covariance matrix of $\hat{\boldsymbol{\Psi}}$ given in (39). Taking the inverse of $\mathrm{cov}(\boldsymbol{\Psi}-\hat{\boldsymbol{\Psi}})$ and comparing with $\mathbf{Q}_\beta^{-1}$ leads to $\mathrm{cov}(\boldsymbol{\Psi}-\hat{\boldsymbol{\Psi}})^{-1} - \mathbf{Q}_\beta^{-1} =$

$\mathbf{G}_c^T(\mathbf{G}_e\mathbf{Q}_e\mathbf{G}_e^T+\mathbf{Q}_c)^{-1}\mathbf{G}_c$. Because the right side has symmetric structure and $\mathbf{G}_c$ does not have full column rank, $\mathbf{Q}_\beta - \mathrm{cov}(\boldsymbol{\Psi}-\hat{\boldsymbol{\Psi}})$ is positive semidefinite. In other words, by utilizing the statistical information of the calibration position error, the updated sensor position vector would never be worse than, if not better than, the original one. It can be shown that $\hat{\mathbf{s}}$ does not reach the CRLB accuracy. However, it is sufficient to provide the CRLB accuracy for the source position estimate.

In the next two stages, the improved sensor positions $\hat{\mathbf{s}}$ will be used to compute the unknown source location estimate. The processing in these two stage is summarized below and the readers are referred to [18] for the details.

Second Stage: This stage exploits the RDOA measurements from the unknown source to estimate the source position $\mathbf{u}^o$ and the extra variable $\hat{r}_1^o = \|\mathbf{u}^o - \hat{\mathbf{s}}_1\|$ that is assumed to be unrelated to $\mathbf{u}^o$. The relation between $\mathbf{u}^o$ and $\hat{r}_1^o$ will be used in the third stage to improve accuracy.

The pseudo linear solution equation for the unknown vector $\boldsymbol{\varphi}_1^o = [\mathbf{u}^{oT}, \hat{r}_1^o]^T$ is [18]

$$\boldsymbol{\varepsilon}_1 = \mathbf{h}_1 - \mathbf{G}_1\boldsymbol{\varphi}_1^o \tag{41}$$

where $\boldsymbol{\varepsilon}_1$ denotes the equation error vector, $\mathbf{h}_1 = [r_{21}^2 - \hat{\mathbf{s}}_2^T\hat{\mathbf{s}}_2 + \hat{\mathbf{s}}_1^T\hat{\mathbf{s}}_1, \ldots, r_{M1}^2 - \hat{\mathbf{s}}_M^T\hat{\mathbf{s}}_M + \hat{\mathbf{s}}_1^T\hat{\mathbf{s}}_1]^T$, r_{i1} is the RDOA measurement from the unknown source (see (3a)) and $\hat{\mathbf{s}}_j$, $j = 1,2,\ldots,M$ are the updated sensor positions from (40). $\mathbf{G}_1$ is an $(M-1)\times 4$ matrix whose $(i-1)$th row is $-2[(\hat{\mathbf{s}}_i - \hat{\mathbf{s}}_1)^T,\ r_{i1}], i = 2,3,\ldots,M$. The weighted least squares (WLS) solution to (41) is

$$\boldsymbol{\varphi}_1 = \left(\mathbf{G}_1^T\mathbf{W}_1\mathbf{G}_1\right)^{-1}\mathbf{G}_1^T\mathbf{W}_1\mathbf{h}_1 \tag{42}$$

where $\mathbf{W}_1$ is the weighting matrix defined as

$$\begin{aligned}\mathbf{W}_1 &= \mathrm{E}\left[\boldsymbol{\varepsilon}_1\boldsymbol{\varepsilon}_1^T\right]^{-1} \\ &= \left(\mathbf{B}_1\mathbf{Q}_\alpha\mathbf{B}_1^T + \mathbf{D}_1\cdot\mathrm{cov}(\boldsymbol{\Psi}-\hat{\boldsymbol{\Psi}})\cdot\mathbf{D}_1^T\right)^{-1}.\end{aligned} \tag{43}$$

$\mathbf{Q}_\alpha$ is the covariance matrix of the RDOA measurement vector $\mathbf{r}$ and $\mathrm{cov}(\boldsymbol{\Psi}-\hat{\boldsymbol{\Psi}})$ is given in (39). $\mathbf{B}_1$ is a diagonal matrix equal to $\mathbf{B}_1 = 2\cdot\mathrm{diag}[r_2^o, r_3^o, \ldots, r_M^o]$, where $r_i^o = \|\mathbf{u}^o - \mathbf{s}_i^o\|$. $\mathbf{D}_1$ is an $(M-1)\times 3M$ matrix and its $(i-1)$th row is $2[-r_{i1}^o\boldsymbol{\rho}_{\mathbf{u}^o,\hat{\mathbf{s}}_1}^T - (\mathbf{u}^o - \hat{\mathbf{s}}_1)^T, \mathbf{0}_{3(i-2)\times 1}^T, (\mathbf{u}^o - \hat{\mathbf{s}}_i)^T,\ \mathbf{0}_{3(M-i)\times 1}^T]$, where r_{i1}^o is the true RDOA given in (4). Under the condition that both the RDOA measurement noise and the errors in the updated sensor positions are sufficiently small, the covariance matrix of $\boldsymbol{\varphi}_1$ is $\mathrm{cov}(\boldsymbol{\varphi}_1) = (\mathbf{G}_1^T\mathbf{W}_1\mathbf{G}_1)^{-1}$.

Third Stage: Exploring the functional relationship between $\mathbf{u}^o$ and $\hat{r}_1^o$ results in the following solution equation for the unknown vector $\boldsymbol{\varphi}_2^o = (\mathbf{u}^o - \hat{\mathbf{s}}_1)\odot(\mathbf{u}^o - \hat{\mathbf{s}}_1)$:

$$\begin{aligned}\boldsymbol{\varepsilon}_2 &= \mathbf{h}_2 - \mathbf{G}_2\boldsymbol{\varphi}_2^o \\ &= \begin{bmatrix}(\boldsymbol{\varphi}_1(1:3) - \hat{\mathbf{s}}_1)\odot(\boldsymbol{\varphi}_1(1:3) - \hat{\mathbf{s}}_1) \\ \boldsymbol{\varphi}_1(4)^2\end{bmatrix} - \begin{bmatrix}\mathbf{I}_{3\times 3} \\ \mathbf{1}_{3\times 1}^T\end{bmatrix}\boldsymbol{\varphi}_2^o\end{aligned} \tag{44}$$

where $\odot$ represents the element by element multiplication and $\mathbf{1}_{3\times 1}$ is a three-by-one vector of unity. Applying again the WLS minimization to (44) yields the solution

$$\boldsymbol{\varphi}_2 = \left(\mathbf{G}_2^T\mathbf{W}_2\mathbf{G}_2\right)^{-1}\mathbf{G}_2^T\mathbf{W}_2\mathbf{h}_2 \tag{45}$$

where the weighting matrix $\mathbf{W}_2$ is

$$\mathbf{W}_2 = \mathrm{E}\left[\boldsymbol{\varepsilon}_2\boldsymbol{\varepsilon}_2^T\right]^{-1} = \mathbf{B}_2^{-T}\left(\mathbf{G}_1^T\mathbf{W}_1\mathbf{G}_1\right)\mathbf{B}_2^{-1} \tag{46}$$

and $\mathbf{B}_2 = 2\cdot\mathrm{diag}[(\mathbf{u}^o - \hat{\mathbf{s}}_1)^T, \hat{r}_1^o]$. The covariance matrix of $\boldsymbol{\varphi}_2$ is $\mathrm{cov}(\boldsymbol{\varphi}_2) = (\mathbf{G}_2^T\mathbf{W}_2\mathbf{G}_2)^{-1}$.

The source location estimate $\mathbf{u}$ is obtained by re-mapping $\boldsymbol{\varphi}_2$ into $\mathbf{u}$ using

$$\mathbf{u} = \mathrm{diag}[\mathrm{sign}(\boldsymbol{\varphi}_1(1:3) - \hat{\mathbf{s}}_1)]\sqrt{\boldsymbol{\varphi}_2} + \hat{\mathbf{s}}_1 \tag{47}$$

where $\mathrm{sign}(\star)$ is the sign function and the diagonal matrix $\mathrm{diag}[\mathrm{sign}(\boldsymbol{\varphi}_1(1:3) - \hat{\mathbf{s}}_1)]$ is used to eliminate the sign ambiguity due to the square-root operation. The covariance matrix of $\mathbf{u}$ is

$$\mathrm{cov}(\mathbf{u}) = \mathbf{B}_3^{-1}\left(\mathbf{G}_2^T\mathbf{W}_2\mathbf{G}_2\right)^{-1}\mathbf{B}_3^{-T} \tag{48}$$

where $\mathbf{B}_3 = 2\cdot\mathrm{diag}[\mathbf{u}^o - \hat{\mathbf{s}}_1]$.

To summarize, the unknown source location estimate $\mathbf{u}$ is obtained by evaluating sequentially (38), (40), (42), (45) and (47). Note that the weighting matrices $\mathbf{W}_1$ and $\mathbf{W}_2$ depend on the true source location $\mathbf{u}^o$ and the true sensor positions $\mathbf{s}_i^o$ that are not available (see (43) and (46)). These difficulties in the algorithm implementation can be bypassed using the approximated version of $\mathbf{W}_1$ and $\mathbf{W}_2$ [18] and the resultant performance degradation is insignificant.

B. Performance Analysis

We shall investigate the efficiency of the proposed localization algorithm with respect to the CRLB. Instead of comparing with the CRLB directly, it will be more convenient to compare the inverse of the CRLB of the source location $\mathbf{u}^o$ and that of the covariance matrix of $\mathbf{u}$. The CRLB is given in (14). Applying the matrix inversion Lemma [22] and substituting the definitions of $\mathbf{X}$ and $\mathbf{Y}$ in (8a) and (8b) yield

$$\begin{aligned}&\mathrm{CRLB}(\mathbf{u}^o)_c^{-1} \\ &\quad= \left(\frac{\partial\mathbf{r}^o}{\partial\mathbf{u}^o}\right)^T\mathbf{Q}_\alpha^{-1}\left(\frac{\partial\mathbf{r}^o}{\partial\mathbf{u}^o}\right) - \left(\frac{\partial\mathbf{r}^o}{\partial\mathbf{u}^o}\right)^T\mathbf{Q}_\alpha^{-1} \\ &\qquad\times\left(\frac{\partial\mathbf{r}^o}{\partial\mathbf{s}^o}\right)\check{\mathbf{Z}}^{-1}\left(\frac{\partial\mathbf{r}^o}{\partial\mathbf{s}^o}\right)^T\mathbf{Q}_\alpha^{-1}\left(\frac{\partial\mathbf{r}^o}{\partial\mathbf{u}^o}\right)\end{aligned} \tag{49}$$

where $\check{\mathbf{Z}}$ is defined in (13). Following the same approach adopted in the Appendix IV of [18], the inverse of $\mathrm{cov}(\mathbf{u})$ from (48) is

$$\mathrm{cov}(\mathbf{u})^{-1} = \mathbf{G}_3^T\mathbf{Q}_\alpha^{-1}\mathbf{G}_3 - \mathbf{G}_3^T\mathbf{Q}_\alpha^{-1}\mathbf{G}_4\dot{\mathbf{Z}}^{-1}\mathbf{G}_4^T\mathbf{Q}_\alpha^{-1}\mathbf{G}_3 \tag{50}$$

where $\mathbf{G}_3 = \mathbf{B}_1^{-1}\mathbf{G}_1\mathbf{B}_2^{-1}\mathbf{G}_2\mathbf{B}_3$, $\mathbf{G}_4 = \mathbf{B}_1^{-1}\mathbf{D}_1$ and

$$\dot{\mathbf{Z}} = \mathbf{Q}_\beta^{-1} + \mathbf{G}_4^T\mathbf{Q}_\alpha^{-1}\mathbf{G}_4 + \mathbf{G}_c^T\left(\mathbf{G}_e\mathbf{Q}_e\mathbf{G}_e^T + \mathbf{Q}_c\right)^{-1}\mathbf{G}_c. \tag{51}$$

Comparing (49) and (50) reveals that $\mathrm{CRLB}(\mathbf{u}^o)_c^{-1}$ and $\mathrm{cov}(\mathbf{u})^{-1}$ have the same structural form. We shall establish their equality using the following two conditions:

C1) $\|\boldsymbol{\Psi}_i\|/\|\mathbf{c}^o - \mathbf{s}_i^o\| \simeq 0$ and $\|\mathbf{e}\|/\|\mathbf{c}^o - \mathbf{s}_i^o\| \simeq 0$, $i = 1,2,\ldots,M$;

C2) $|n_{i1}|/\|\mathbf{u}^o - \mathbf{s}_i^o\| \simeq 0$ and $\|\boldsymbol{\Psi}_i - \hat{\boldsymbol{\Psi}}_i\|/\|\mathbf{u}^o - \mathbf{s}_i^o\| \simeq 0$, $i = 1,2,\ldots,M$.

The first condition indicates that the distance between the calibration emitter and sensor i is much larger than the 2-norms of both the sensor position error $\mathbf{\Psi}_i$ and the calibration position error $\mathbf{e}$. The satisfaction of C1) is required for the validity of the first-order approximation in (34). This can be verified as follows. Note that (34) is valid if $\|\mathbf{\Psi}_i\|/\|\mathbf{c}-\mathbf{s}_i\| \simeq 0$ and $\|\mathbf{e}\|/\|\mathbf{c}-\mathbf{s}_i\| \simeq 0, i = 1, 2, \ldots, M$. They are true if C1) is satisfied, because under C1), we have, after substituting (1) and (2),

$$\begin{aligned}\|\mathbf{c}-\mathbf{s}_i\| &\simeq \|\mathbf{c}^o-\mathbf{s}_i^o\| \\ &\quad\cdot\sqrt{1-2\boldsymbol{\rho}_{\mathbf{c}^o,\mathbf{s}_i^o}^T\frac{\mathbf{\Psi}_i}{\|\mathbf{c}^o-\mathbf{s}_i^o\|}+2\boldsymbol{\rho}_{\mathbf{c}^o,\mathbf{s}_i^o}^T\cdot\frac{\mathbf{e}}{\|\mathbf{c}^o-\mathbf{s}_i^o\|}} \\ &\simeq \|\mathbf{c}^o-\mathbf{s}_i^o\|. \end{aligned} \tag{52}$$

The condition C2) implies that the RDOA measurement noise and the error in the updated sensor positions $\hat{\mathbf{s}}_i$ are small relative to the distance between the unknown source and the ith sensor.

Under C1) and C2), Appendix V in [18] has shown that $\mathbf{G}_3 \simeq (\partial\mathbf{r}^o/\partial\mathbf{u}^o)$, $\mathbf{G}_4 \simeq -(\partial\mathbf{r}^o/\partial\mathbf{s}^o)$ and $\mathbf{G}_c \simeq -(\partial\tilde{\mathbf{r}}^o/\partial\mathbf{s}^o)$. Putting these results into (50) and comparing with (49) reveals that the difference between $\mathrm{CRLB}(\mathbf{u}^o)_c^{-1}$ and $\mathrm{cov}(\mathbf{u})^{-1}$ is $(\partial\tilde{\mathbf{r}}^o/\partial\mathbf{c}^o)$ versus $\mathbf{G}_e$. Applying the condition C1), Appendix V proves that

$$\mathbf{G}_e \simeq -\left(\frac{\partial\tilde{\mathbf{r}}^o}{\partial\mathbf{c}^o}\right). \tag{53}$$

Therefore, we obtain

$$\mathrm{cov}(\mathbf{u})^{-1} \simeq \mathrm{CRLB}(\mathbf{u}^o)_c^{-1}.$$

In other words, the proposed three-stage algorithm can achieve the CRLB accuracy and therefore is an efficient estimator of the unknown source location, when the conditions C1) and C2) are satisfied. In practice, C1) and C2) can be fulfilled if both the unknown source and the calibration emitter are distant from the sensor array, and the measurement noise, sensor position error and calibration position error are moderate. For sources that are close to the sensor array, these conditions are still valid if the measurement noise and the position errors in the sensors and calibration emitter are sufficiently small.

VI. Source Localization With Multiple Calibration Emitters

So far our study focuses on a single calibration emitter for the purpose of simplifying the illustration. This section presents the results when multiple calibration emitters are available. We shall re-examine the CRLB of the source location and derive the conditions under which the effect of sensor position error on the source localization accuracy can be completely removed through the use of multiple calibration emitters. Then, the generalization of the localization algorithm developed in Section V-A to the multiple calibration emitter scenario will be described. Finally, a brief performance evaluation of the generalized solution with respect to the CRLB will be given.

A. CRLB Analysis

The CRLB result in Section III, although derived for the single calibration emitter scenario, is also valid for $N(>1)$ calibration emitters. The CRLB is in (14), where $\mathbf{X}$, $\mathbf{Y}$ and $\check{\mathbf{Z}}$ are given in (8a), (8b), and (13). In (13), $\tilde{\mathbf{r}}^o$ is now $N(M-1)\times 1$ as defined under (5), $\mathbf{c}^o$ is $3N\times 1$ as defined under (2) and the covariance matrices $\mathbf{Q}_c$ and $\mathbf{Q}_e$ are $N(M-1)\times N(M-1)$ and $3N\times 3N$. Also, the Jacobian matrices $(\partial\tilde{\mathbf{r}}^o/\partial\mathbf{s}^o)$ and $(\partial\tilde{\mathbf{r}}^o/\partial\mathbf{c}^o)$ in $\check{\mathbf{Z}}$ have $N(M-1)$ rows and from (5), their $((j-1)(M-1)+(i-1))$th rows are

$$\left(\frac{\partial\tilde{r}_{i1,j}^o}{\partial\mathbf{s}^o}\right) = \left[\boldsymbol{\rho}_{\mathbf{c}_j^o,\mathbf{s}_1^o}^T,\ \underbrace{\mathbf{0}^T}_{1\times 3(i-2)},\ -\boldsymbol{\rho}_{\mathbf{c}_j^o,\mathbf{s}_i^o}^T,\ \underbrace{\mathbf{0}^T}_{1\times 3(M-i)}\right] \tag{54a}$$

$$\left(\frac{\partial\tilde{r}_{i1,j}^o}{\partial\mathbf{c}^o}\right) = \left[\underbrace{\mathbf{0}^T}_{1\times 3(j-1)},\ \boldsymbol{\rho}_{\mathbf{c}_j^o,\mathbf{s}_i^o}^T-\boldsymbol{\rho}_{\mathbf{c}_j^o,\mathbf{s}_1^o}^T,\ \underbrace{\mathbf{0}^T}_{1\times 3(N-j)}\right] \tag{54b}$$

where $i = 2, 3, \ldots, M$ and $j = 1, 2, \ldots, N$. Same as in the single calibration emitter case, the first term in the CRLB (14) is the lower bound when the true sensor positions are exactly known and the second term is the increase in the bound due to the sensor and calibration position errors. It can be shown that $\check{\mathbf{Z}}$ increases with N. Thus, having more calibration emitters can improve the source localization accuracy. We next examine the possibility of completely eliminating the effect of sensor position error on the source localization accuracy. Mathematically, it is equivalent to require that the second term on the right of (14) is near zero. We shall show below two solutions to make this happen by making $\check{\mathbf{Z}}$ tend to infinity. The first solution is very difficult to achieve in practice and the second solution is more practical.

The first solution requires that 1) $N \geq 4$, 2) $\mathbf{c}_j^o \neq \mathbf{c}_k^o$, for all $j \neq k$, $j = 1, 2, \ldots, N$, $k = 1, 2, \ldots, N$ and all calibration emitters together are not coplanar with any sensor, and 3) $\mathbf{Q}_c \to \mathbf{O}$ and $\mathbf{Q}_e \to \mathbf{O}$. The conditions 1) and 2) guarantee that $(\partial\tilde{\mathbf{r}}^o/\partial\mathbf{s}^o)$, which is $N(M-1)\times 3M$, has full column rank of $3M$ and the third term of $\check{\mathbf{Z}}$ is not rank deficient. Condition 3) increases the third term in $\check{\mathbf{Z}}$ to infinity. In other words, we can completely remove the sensor position error if there are at least 4 calibration emitters at distinct locations not lying in the same plane, the calibration emitter positions and the calibration RDOAs are noise free. The intuition behind is that with the noiseless calibration RDOAs, at least $4(M-1)(\geq 3M)$ RDOA equations parameterized on the sensor positions can be constructed using (5) and as such, the $3M\times 1$ true sensor position vector $\mathbf{s}^o$ can be uniquely identified. The resultant source location accuracy then becomes unaffected by the sensor position error.

The second solution demands that 1) $N \to +\infty$ and 2) the number of distinct calibration emitter positions is no less than 4 and all calibration emitters together are not coplanar with any sensor. Condition 1) makes the third term in $\check{\mathbf{Z}}$, which is indeed in quadratic inner product form, become an infinitely large matrix, while condition 2) renders it invertible. The second solution indicates that even when the true calibration emitter positions are not known and the calibration RDOAs are noisy ($\mathbf{Q}_e \neq \mathbf{O}$

and $\mathbf{Q}_c \neq \mathbf{O}$), the sensor position error can still be eliminated, if there is sufficiently large number of calibration emitters not lying in the same plane and they are located at no less than four different positions. The underlying reason for completely removing the sensor position error is that each calibration emitter, although it has position uncertainty, can contribute to some degree of correction in the sensor positions and improvement in the source localization accuracy. Hence, when the number of calibration emitters N goes to infinity, we would gather sufficient knowledge to mitigate the sensor position error to such an extent that the localization accuracy of the unknown source will reach $\mathrm{CRLB}(\mathbf{u}^o)$.

B. Localization Algorithm

We shall extend the algorithm presented in Section V-A to exploit the RDOA measurements from the N calibration emitters to improve the source location estimate. Only the first stage of the proposed algorithm needs to be modified, while the processing of the second and third stages remains unchanged.

In the presence of multiple calibration emitters, the estimate of the sensor position error vector $\mathbf{\Psi}$ obtained in the first stage has the same functional form as in (38), where $\mathbf{h}_c$ is $N(M-1)\times 1$ and its $((j-1)(M-1)+(i-1))$th element, $i=2,3,\ldots,M$, $j=1,2,\ldots,N$, is $\tilde{r}_{i1,j}-\hat{r}_{i1,j}$. $\tilde{r}_{i1,j}$ is the measured RDOA between sensor pair i and 1 from the jth calibration emitter (see (3b)). $\hat{r}_{i1,j}=\|\mathbf{c}_j-\mathbf{s}_i\|-\|\mathbf{c}_j-\mathbf{s}_1\|$ is the predicted version of $\tilde{r}_{i1,j}$ and it is obtained using the available inaccurate location of the jth calibration emitter and the erroneous sensor positions. $\mathbf{G}_c$ and $\mathbf{G}_e$ are $N(M-1)\times 3M$ and $N(M-1)\times 3N$, and their $((j-1)(M-1)+(i-1))$th rows are

$$\mathbf{G}_c[(j-1)(M-1)+(i-1),:] = \left[-\boldsymbol{\rho}^T_{\mathbf{c}_j,\mathbf{s}_1},\ \underbrace{\mathbf{0}^T}_{1\times 3(i-2)},\ \boldsymbol{\rho}^T_{\mathbf{c}_j,\mathbf{s}_i},\ \underbrace{\mathbf{0}^T}_{1\times 3(M-i)}\right] \tag{55a}$$

$$\mathbf{G}_e[(j-1)(M-1)+(i-1),:] = \left[\underbrace{\mathbf{0}^T}_{1\times 3(j-1)},\ \boldsymbol{\rho}^T_{\mathbf{c}_j,\mathbf{s}_1}-\boldsymbol{\rho}^T_{\mathbf{c}_j,\mathbf{s}_i},\ \underbrace{\mathbf{0}^T}_{1\times 3(N-j)}\right]. \tag{55b}$$

With the estimate of the sensor position error vector, we can update sensor position vector using (40). Then, sequentially evaluating (42), (45), and (47) using the updated sensor position vector and the RDOA measurements from the unknown source would yield the desired source location estimate $\mathbf{u}$.

C. Performance Evaluation

Performance analysis follows the same approach as in Section V-B by comparing the inverse of the CRLB and that of the source location covariance matrix $\mathrm{cov}(\mathbf{u})$. The CRLB inverse is given in (49). The covariance inverse is given in (50). (49) and (50) have the relevant quantities $\tilde{\mathbf{r}}^o$, $\mathbf{c}^o$, $\mathbf{Q}_c$, $\mathbf{Q}_e$, $\mathbf{G}_c$ (see (55a)), and $\mathbf{G}_e$ (see (55b)) defined for N calibration emitters. After using the same algebraic manipulations as in Section V-B, it can be shown that the proposed solution reaches the CRLB accuracy under the conditions C1) (after being extended to the N calibration emitter case) and C2).

Note that the current work does not consider estimating the calibration emitter positions because we are interested in determining the unknown source position $\mathbf{u}^o$ only. The joint estimation of $\mathbf{u}^o$ together with sensor and calibration positions is feasible. Nevertheless, compared to the proposed solution, we do not expect that the joint estimation would necessarily lead to improved source location estimates when the noise level is small. In fact, as the theoretical analysis in this subsection shows, the proposed algorithm achieves the CRLB accuracy under two mild conditions.

The present study implicitly assumes that the calibration emitters do not provide TDOA measurements of the unknown source. If this is not the case, we may expect by intuition that a localization algorithm that jointly utilizes the TDOA measurements obtained at the receiving sensors and calibration emitters would provide better source localization accuracy than the method proposed in this paper that uses the TDOAs at the receiving sensors only. Further study of this problem is beyond the scope of this paper. This is an interesting research problem for future investigation.

VII. Simulations

We shall verify through simulations the efficiency of the localization algorithms developed in Sections V-A and VI-B, and the validity of the second method proposed in Section VI-A for completely removing the effect of sensor position error. The simulation scenario contains a distant unknown source located at $\mathbf{u}^o=[2000,2500,3000]^T$ m and the localization task is performed by an array of $M=6$ receiving sensors. The actual sensor positions are given in Table I. The localization accuracy from simulation is calculated using $\mathrm{MSE}(\mathbf{u})=\sum_{l=1}^{L}\|\mathbf{u}_l-\mathbf{u}^o\|^2/L$, where $\mathbf{u}_l$ is the source location estimate at ensemble l and $L=10^4$ is the number of ensemble runs. In generating the simulation results, the RDOA measurements from the unknown source and $N(\geq 1)$ calibration emitters are produced via adding to the true values zero mean Gaussian noise with covariance matrices $\mathbf{Q}_\alpha=\sigma_r^2\mathbf{J}$ and $\mathbf{Q}_c=\sigma_r^2\tilde{\mathbf{J}}$, where σ_r^2 is set to be 10^{-3}. $\mathbf{J}$ is an $(M-1)\times(M-1)$ matrix whose diagonal elements are 1 and all other elements are 0.5 [16]. $\tilde{\mathbf{J}}$ is an $N(M-1)\times N(M-1)$ block diagonal matrix and its diagonal blocks are equal to $\mathbf{J}$. The erroneous sensor and calibration emitter positions are created in a similar way using covariance matrices $\mathbf{Q}_\beta=\sigma_s^2\mathbf{I}_{3M\times 3M}$ and $\mathbf{Q}_e=\sigma_e^2\mathbf{I}_{3N\times 3N}$. The sensor position noise power σ_s^2 is fixed at -20 in log scale in all simulations.

Fig. 6 gives the localization accuracy of the solution proposed in Section V-A when a single calibration emitter with position uncertainty is present. For the purpose of comparison, we also plot the minimum achievable localization MSE, the trace of $\mathrm{CRLB}(\mathbf{u}^o)_c$ from (10). Fig. 6(a) shows the results for the case where the calibration emitter is positioned at $\mathbf{c}_1^o=[1500,1550,1500]^T$ m that is farther away from the sensor array. Fig. 6(b) depicts the results when the calibration emitter is deployed at $\mathbf{c}_1^o=[450,125,300]^T$ m that is closer to the sensor array. In both cases, the proposed solution is able to achieve the CRLB accuracy when the calibration position noise power is not large ($\sigma_e^2/\sigma_s^2\leq 35$ dB). As σ_e^2/σ_s^2 further increases, the simulation MSE starts to deviate from the CRLB.

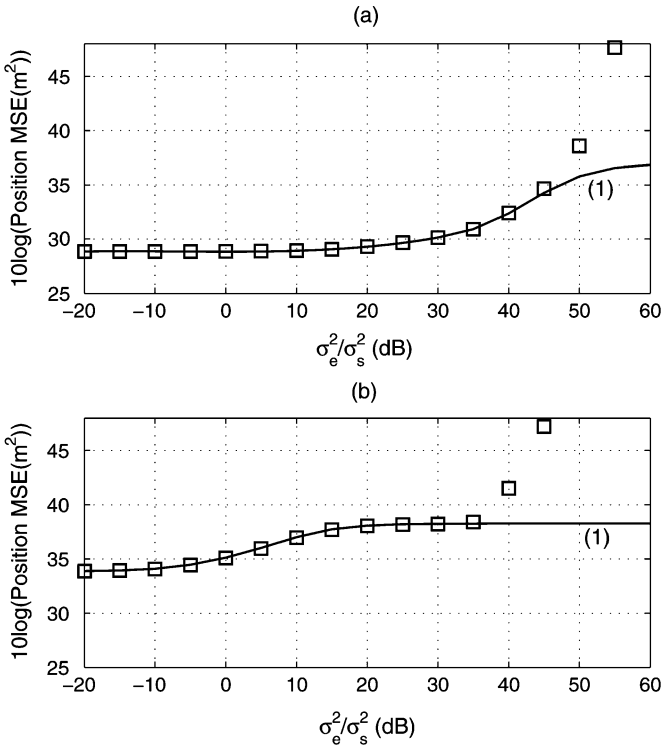

Fig. 6. Comparison of the CRLB of $\mathbf{u}^o$ and the localization accuracy of the proposed solution in Section V-A in the single calibration emitter scenario. (a) Calibration emitter farther away from the sensor array. (b) Calibration emitter closer to the sensor array. (1) $\mathrm{tr}(\mathrm{CRLB}(\mathbf{u}^o)_c)$ from (10), simulation MSE from the proposed solution: square symbol.

This is mainly because the 2-norm of the calibration position error now becomes comparable to the range between the calibration emitter and the sensor. As a result, the condition C1) stated in Section V-B is violated and the proposed localization algorithm can no longer attain the CRLB performance.

Fig. 7 examines the performance of the solution developed in Section VI-B. Two calibration emitters are used (i.e., $N = 2$) and they are located at $\mathbf{c}_1^o = [1500, 1550, 1500]^T$ m and $\mathbf{c}_2^o = [1000, 1500, 1550]^T$ m. Similar to the observation from Fig. 6, the proposed algorithm is able to reach the CRLB accuracy before the calibration position noise power becomes sufficiently big ($\sigma_e^2/\sigma_s^2 \geq 45$ dB). This is in fact an expected result from the analysis in Section VI-C. Moreover, by comparing Fig. 7 with Fig. 6(a), we can notice that the use of two calibration emitters $\mathbf{c}_1^o$ and $\mathbf{c}_2^o$ leads to a better source localization accuracy over the case where only $\mathbf{c}_1^o$ is available. For instance, when σ_e^2/σ_s^2 is equal to 30 dB, using two calibration emitters can improve the accuracy by 2 dB.

Fig. 8 plots the trace of the CRLB of the source location estimate with multiple calibration emitters as a function of $\log_2(N)$. We also depict the trace of $\mathrm{CRLB}(\mathbf{u}^o)$, the best localization accuracy when the true sensor positions are known exactly, and the localization MSE of the solution presented in Section VI-B. Two sets of results are given and they correspond to the calibration position noise power σ_e^2 equal to -10 and 10 in log scale. To simplify the simulation process, each calibration emitter will have one of the following four positions: $\mathbf{p}_1^o = [1500, 1550, 1500]^T$ m, $\mathbf{p}_2^o = [1000, 1250, 1500]^T$ m,

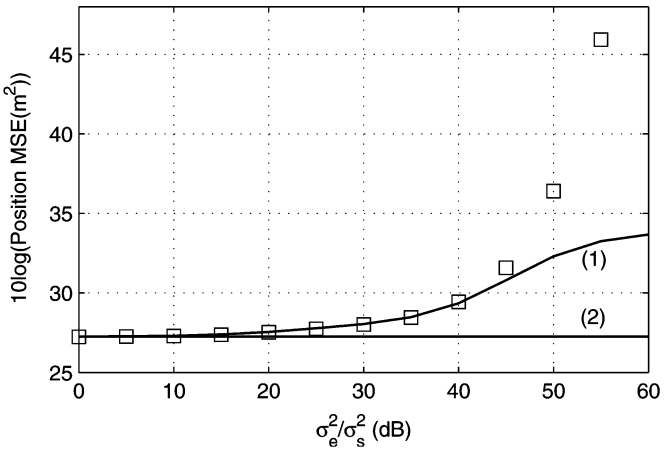

Fig. 7. Comparison of the CRLBs of $\mathbf{u}^o$ and the source localization accuracy of the proposed solution in Section VI-B in the two calibration emitter scenario. (1) $\mathrm{tr}(\mathrm{CRLB}(\mathbf{u}^o)_c)$ from (14), simulation MSE from the proposed solution: square symbol, (2) $\mathrm{tr}(\mathrm{CRLB}(\mathbf{u}^o)_{c^o})$ from (11).

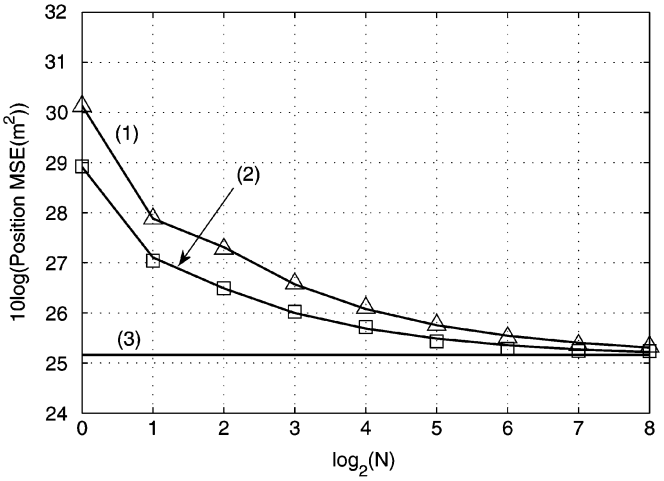

Fig. 8. Removal of the effect of sensor position error on source localization accuracy using multiple calibration emitters with position errors. (1) $\mathrm{tr}(\mathrm{CRLB}(\mathbf{u}^o)_c)$ from (14) evaluated at $\sigma_e^2 = 10$ in log scale, simulation MSE from the proposed solution in Section VI-B: triangle symbol, (2) $\mathrm{tr}(\mathrm{CRLB}(\mathbf{u}^o)_c)$ from (14) evaluated at $\sigma_e^2 = -10$ in log scale, simulation MSE from the proposed solution in Section VI-B: square symbol, (3) $\mathrm{tr}(\mathrm{CRLB}(\mathbf{u}^o))$.

$\mathbf{p}_3^o = [1550, 1000, 1500]^T$ m, and $\mathbf{p}_4^o = [600, 750, 750]^T$ m. The true calibration position vector $\mathbf{c}^o$ is set as

$$\mathbf{c}^o = \Big[\underbrace{\mathbf{p}_1^{oT}, \ldots, \mathbf{p}_1^{oT}}_{1\times 3j}, \underbrace{\mathbf{p}_2^{oT}, \ldots, \mathbf{p}_2^{oT}}_{1\times 3j}, \underbrace{\mathbf{p}_3^{oT}, \ldots, \mathbf{p}_3^{oT}}_{1\times 3j}, \underbrace{\mathbf{p}_4^{oT}, \ldots, \mathbf{p}_4^{oT}}_{1\times 3j}, \underbrace{\mathbf{p}_1^{oT}, \ldots, \mathbf{p}_i^{oT}}_{1\times 3i}\Big]^T$$

where $j = \lfloor (N/4) \rfloor$ and $i = N - 4j$. The symbol $\lfloor \star \rfloor$ denotes the floor operation.

We can see from Fig. 8 that as N increases, the lower bound for the source location MSE in the presence of position errors

in both the sensor and calibration emitters gradually approaches the one without sensor position error. This observation indicates that the effect of sensor position error on the source location estimate can be removed by deploying a large number of calibration emitters at no less than four distinct locations. It can also be noticed that the lower bound with a smaller calibration position noise power σ_e^2 (curve (2)) converges to the value of $\mathrm{tr}(\mathrm{CRLB}(\mathbf{u}^o))$ faster than the bound with a larger value of σ_e^2 (curve (1)). This can be explained using the discussion below (14) that the calibration position error affects the source localization accuracy via increasing the calibration RDOA noise. With a larger calibration position noise power, more calibration emitters are needed to reduce the effect of the calibration RDOA noise so that the sensor positions can be precisely estimated. Finally, it is evident from the figure that the solution developed in Section VI-B attains the CRLB accuracy. In other words, with the proposed closed-form solution in Section VI-B, the improvement in the best source localization accuracy due to the use of multiple calibration emitters is indeed achievable.

VIII. Conclusion

This paper investigated the use of calibration emitters whose positions are not known exactly to improve the TDOA source localization accuracy in the presence of sensor position uncertainty. We started our study by considering the simpler case where only one calibration emitter is available. The CRLB of the source location for this scenario was evaluated and the loss in accuracy due to calibration position error was established. When comparing with the CRLB without using a calibration emitter, we found that using a calibration emitter can always provide improvement, even when the calibration position is completely unknown, a finding consistent with previous study on the Bayesian sensor network localization. The paper then performed a first-order analysis of a pseudo ML estimator that assumes the calibration emitter position is accurate but in fact has error. The analysis result indicates that the source localization accuracy could be very sensitive to the calibration position error. We continued to propose a closed-form algorithm based on the one developed in [18] to take the statistical knowledge of the calibration position error into account. The new solution was shown analytically to reach the CRLB accuracy, when two mild conditions are met. Finally, the paper studied the localization scenario where an arbitrary number of calibration emitters at inaccurate positions are used in the localization task. The CRLB of the source location was re-examined, the proposed localization algorithm was generalized by exploiting all calibration TDOA measurements and its performance was also shown analytically to reach the CRLB under similar conditions as in the single calibration emitter case. Two possible scenarios were presented under which the effect of sensor position error on the source localization accuracy can be completely eliminated by taking the advantage of having multiple calibration emitters. The theoretical derivations and the performance of the proposed localization algorithms were verified by simulations.

Appendix I
Symbols and Notations

The symbols and notations used are summarized in Table II.

Appendix II
Proof of (10)

We begin with partitioning the FIM in (7) as

$$\mathrm{FIM} = \begin{bmatrix} \mathbf{X} & \bar{\mathbf{Y}} \\ \bar{\mathbf{Y}}^T & \bar{\mathbf{Z}} \end{bmatrix} \tag{56}$$

where $\bar{\mathbf{Y}} = [\mathbf{Y}\ \mathbf{O}]$ and

$$\bar{\mathbf{Z}} = \begin{bmatrix} \mathbf{Z} & \mathbf{R}^T \\ \mathbf{R} & \mathbf{P} \end{bmatrix}.$$

Applying the partitioned matrix inverse formula [22] to (56) and denoting the upper left three-by-three block as $\mathrm{CRLB}(\mathbf{u}^o)_c$, we arrive at

$$\begin{aligned}\mathrm{CRLB}(\mathbf{u}^o)_c &= (\mathbf{X} - \bar{\mathbf{Y}}\bar{\mathbf{Z}}^{-1}\bar{\mathbf{Y}}^T)^{-1} = \mathbf{X}^{-1} \\ &\quad + \mathbf{X}^{-1}\bar{\mathbf{Y}}\left(\bar{\mathbf{Z}} - \bar{\mathbf{Y}}^T\mathbf{X}^{-1}\bar{\mathbf{Y}}\right)^{-1}\bar{\mathbf{Y}}^T\mathbf{X}^{-1}. \end{aligned} \tag{57}$$

The middle part of the second term in (57) is a quadratic form in $\bar{\mathbf{Y}}$, and it is equal to, after substituting the definition of $\bar{\mathbf{Y}}$ and $\bar{\mathbf{Z}}$,

$$\begin{aligned}&\bar{\mathbf{Y}}(\bar{\mathbf{Z}} - \bar{\mathbf{Y}}^T\mathbf{X}^{-1}\bar{\mathbf{Y}})^{-1}\bar{\mathbf{Y}}^T \\ &\quad = [\mathbf{Y} \quad \mathbf{O}]\begin{bmatrix} \mathbf{Z} - \mathbf{Y}^T\mathbf{X}^{-1}\mathbf{Y} & \mathbf{R}^T \\ \mathbf{R} & \mathbf{P} \end{bmatrix}^{-1}\begin{bmatrix} \mathbf{Y}^T \\ \mathbf{O} \end{bmatrix}. \end{aligned} \tag{58}$$

Applying the partitioned matrix inverse formula [22] to the big matrix in the middle simplifies the above quadratic form to

$$\begin{aligned}&\bar{\mathbf{Y}}(\bar{\mathbf{Z}} - \bar{\mathbf{Y}}^T\mathbf{X}^{-1}\bar{\mathbf{Y}})^{-1}\bar{\mathbf{Y}}^T \\ &\quad = \mathbf{Y}(\mathbf{Z} - \mathbf{Y}^T\mathbf{X}^{-1}\mathbf{Y} - \mathbf{R}^T\mathbf{P}^{-1}\mathbf{R})^{-1}\mathbf{Y}^T. \end{aligned} \tag{59}$$

Substituting (59) back into (57) yields (10).

Appendix III

Substituting the definitions of $\mathbf{P}$ in (8e) and $\mathbf{R}$ in (8d) into $\mathbf{P} - \mathbf{R}\mathbf{B}^{-1}\mathbf{R}^T$ and simplifying yield

$$\begin{aligned}&\mathbf{P} - \mathbf{R}\mathbf{B}^{-1}\mathbf{R}^T \\ &\quad = \mathbf{Q}_e^{-1} + \left(\frac{\partial\tilde{\mathbf{r}}^o}{\partial\mathbf{c}^o}\right)^T\left[\mathbf{Q}_c^{-1} - \mathbf{Q}_c^{-1}\left(\frac{\partial\tilde{\mathbf{r}}^o}{\partial\mathbf{s}^o}\right)\right. \\ &\qquad \left.\times\ \mathbf{B}^{-1}\left(\frac{\partial\tilde{\mathbf{r}}^o}{\partial\mathbf{s}^o}\right)^T\mathbf{Q}_c^{-1}\right]\left(\frac{\partial\tilde{\mathbf{r}}^o}{\partial\mathbf{c}^o}\right). \end{aligned} \tag{60}$$

The matrix $\mathbf{B}$ is defined under (12) and it is equal to $\mathbf{Z} - \mathbf{Y}^T\mathbf{X}^{-1}\mathbf{Y}$. If we express $\mathbf{Z}$ given in (8c) as $\mathbf{Z} = \hat{\mathbf{Z}} + (\partial\tilde{\mathbf{r}}^o/\partial\mathbf{s}^o)^T\mathbf{Q}_c^{-1}(\partial\tilde{\mathbf{r}}^o/\partial\mathbf{s}^o)$, where $\hat{\mathbf{Z}} = \mathbf{Q}_\beta^{-1} + (\partial\mathbf{r}^o/\partial\mathbf{s}^o)^T\mathbf{Q}_\alpha^{-1}(\partial\mathbf{r}^o/\partial\mathbf{s}^o)$, $\mathbf{B}$ can then be rewritten as

$$\mathbf{B} = (\hat{\mathbf{Z}} - \mathbf{Y}^T\mathbf{X}^{-1}\mathbf{Y}) + \left(\frac{\partial\tilde{\mathbf{r}}^o}{\partial\mathbf{s}^o}\right)^T\mathbf{Q}_c^{-1}\left(\frac{\partial\tilde{\mathbf{r}}^o}{\partial\mathbf{s}^o}\right). \tag{61}$$

TABLE II
SYMBOLS AND NOTATIONS

Symbol	Explanation
M	number of sensors
N	number of calibration emitters
$(\star)^o$	true value of the noisy quantity $(\star)$
$\mathbf{u}^o$	position of the unknown source, $\mathbf{u}^o = [x_u^o, y_u^o, z_u^o]^T$
$\mathbf{s}_i$	noisy position of the ith sensor, $\mathbf{s}_i = [x_{s,i}, y_{s,i}, z_{s,i}]^T$
$\mathbf{c}_j$	noisy position of the jth calibration emitter, $\mathbf{c}_j = [x_{c,j}, y_{c,j}, z_{c,j}]^T$
$\mathbf{\Psi}_i$	position error vector of the ith sensor so that $\mathbf{s}_i = \mathbf{s}_i^o + \mathbf{\Psi}_i$
$\mathbf{e}_j$	position error vector of the jth calibration emitter so that $\mathbf{c}_j = \mathbf{c}_j^o + \mathbf{e}_j$
$\mathbf{s}$	$3M \times 1$ sensor position vector, $\mathbf{s} = [\mathbf{s}_1^T, \mathbf{s}_2^T, ..., \mathbf{s}_M^T]^T$
$\mathbf{\Psi}$	$3M \times 1$ sensor position error vector, $\mathbf{\Psi} = [\mathbf{\Psi}_1^T, \mathbf{\Psi}_2^T, \ldots, \mathbf{\Psi}_M^T]^T$
$\mathbf{c}$	$3N \times 1$ calibration position vector, $\mathbf{c} = [\mathbf{c}_1^T, \mathbf{c}_2^T, ..., \mathbf{s}_N^T]^T$
$\mathbf{e}$	$3N \times 1$ calibration position error vector, $\mathbf{e} = [\mathbf{e}_1^T, \mathbf{e}_2^T, \ldots, \mathbf{e}_N^T]^T$
r_i^o	true distance between the unknown source and sensor i
$\tilde{r}_{i,j}^o$	true distance between the jth calibration emitter and sensor i
r_{i1}	RDOA measurement from $\mathbf{u}^o$ between sensor pair i and 1
n_{i1}	measurement noise in r_{i1} so that $r_{i1} = r_{i1}^o + n_{i1}$
$\tilde{r}_{i1,j}$	RDOA measurement from the jth calibration emitter between sensor pair i and 1
$\tilde{n}_{i1,j}$	measurement noise in $\tilde{r}_{i1,j}$ so that $\tilde{r}_{i1,j} = \tilde{r}_{i1,j}^o + \tilde{n}_{i1,j}$
$\mathbf{r}$	$(M-1) \times 1$ RDOA measurement vector from $\mathbf{u}^o$, $\mathbf{r} = [r_{21}, r_{31}, ..., r_{M1}]^T$
$\mathbf{n}$	$(M-1) \times 1$ RDOA measurement noise vector of $\mathbf{r}$ so that $\mathbf{r} = \mathbf{r}^o + \mathbf{n}$
$\tilde{\mathbf{r}}$	$N(M-1) \times 1$ calibration RDOA measurement vector, $\tilde{\mathbf{r}} = [\tilde{r}_{21,1}, \tilde{r}_{31,1}, ..., \tilde{r}_{M1,1}, \tilde{r}_{21,2}, ..., \tilde{r}_{M1,N}]^T$
$\tilde{\mathbf{n}}$	$N(M-1) \times 1$ RDOA measurement noise vector of $\tilde{\mathbf{r}}$ so that $\tilde{\mathbf{r}} = \tilde{\mathbf{r}}^o + \tilde{\mathbf{n}}$
$\mathbf{Q}_\alpha$	$(M-1) \times (M-1)$ covariance matrix of $\mathbf{r}$, i.e., $E[\mathbf{n}\mathbf{n}^T]$
$\mathbf{Q}_\beta$	$3M \times 3M$ covariance matrix of $\mathbf{s}$, i.e., $E[\mathbf{\Psi}\mathbf{\Psi}^T]$
$\mathbf{Q}_c$	$N(M-1) \times N(M-1)$ covariance matrix of $\tilde{\mathbf{r}}$, i.e., $E[\tilde{\mathbf{n}}\tilde{\mathbf{n}}^T]$
$\mathbf{Q}_e$	$3N \times 3N$ covariance matrix of $\mathbf{c}$, i.e., $E[\mathbf{e}\mathbf{e}^T]$
$\partial\mathbf{a}/\partial\mathbf{b}$	Jacobian matrix whose ith row is the derivative of the ith element in $\mathbf{a}$ with respect to $\mathbf{b}^T$
$\boldsymbol{\rho}_{\mathbf{a},\mathbf{b}}$	unit vector from $\mathbf{b}$ to $\mathbf{a}$, $\boldsymbol{\rho}_{\mathbf{a},\mathbf{b}} = \frac{\mathbf{a}-\mathbf{b}}{\|\mathbf{a}-\mathbf{b}\|}$
$\mathbf{A}[i,:]$	the ith row of matrix $\mathbf{A}$
$\mathbf{m}$	composite measurement vector, $\mathbf{m} = [\mathbf{r}^T, \tilde{\mathbf{r}}^T, \mathbf{s}^T]^T$
$\mathbf{W}$	covariance matrix of $\mathbf{m}$
$\boldsymbol{\theta}^o$	unknown parameter vector, $\boldsymbol{\theta}^o = [\mathbf{u}^{oT}, \mathbf{s}^{oT}]^T$
$\check{\boldsymbol{\theta}}$	estimate of $\boldsymbol{\theta}^o$ when ignoring the calibration position error, $\check{\boldsymbol{\theta}} = [\check{\mathbf{u}}^T, \check{\mathbf{s}}^T]^T$
$\boldsymbol{\epsilon}$	estimation error of $\check{\boldsymbol{\theta}}$
$\bar{\mathbf{G}}$	gradient matrix of Taylor-series expansion of $\mathbf{m}$
$\hat{\mathbf{\Psi}}$	$3M \times 1$ sensor position error estimate
$\hat{\mathbf{s}}$	$3M \times 1$ improved sensor position vector from calibration RDOA measurements, $\hat{\mathbf{s}} = [\hat{\mathbf{s}}_1^T, \hat{\mathbf{s}}_2^T, ..., \hat{\mathbf{s}}_M^T]^T$
$\mathbf{G}_c$	$N(M-1) \times 3M$ regressor of stage 1 in the proposed algorithm
$\mathbf{G}_e$	$N(M-1) \times 3N$ transformation matrix of calibration position error in stage 1 of the proposed algorithm
$\mathbf{h}_c$	$N(M-1) \times 1$ regressand of stage 1 in the proposed algorithm
$\hat{r}_i^o$	distance between the unknown source $\mathbf{u}^o$ and the improved sensor position $\hat{\mathbf{s}}_i$
$\mathbf{G}_i$	regressor of stage $i+1$, $i = 1, 2$, in the proposed algorithm
$\mathbf{h}_i$	regressand of stage $i+1$, $i = 1, 2$, in the proposed algorithm
$\boldsymbol{\varphi}_i$	solution vector of stage $i+1$, $i = 1, 2$, in the proposed algorithm
$\boldsymbol{\varepsilon}_i$	equation error vector in stage $i+1$, $i = 1, 2$, in the proposed algorithm
$\mathbf{W}_i$	weighting matrix of stage $i+1$, $i = 1, 2$, in the proposed algorithm
CRLB$(\mathbf{u}^o)_c$	CRLB of $\mathbf{u}^o$ with sensor position error and having N calibration emitters at noisy locations
CRLB$(\mathbf{u}^o)_{c^o}$	CRLB of $\mathbf{u}^o$ with sensor position error and having N calibration emitters at exact locations
CRLB$(\mathbf{u}^o)$	CRLB of $\mathbf{u}^o$ without sensor position error
CRLB$(\mathbf{u}^o)_o$	CRLB of $\mathbf{u}^o$ with sensor position error and without calibration emitters
cov$(\check{\mathbf{u}})$	covariance matrix of source location estimate $\check{\mathbf{u}}$ when ignoring the calibration position error
cov$(\mathbf{u})$	covariance matrix of source location estimate $\mathbf{u}$ from the proposed algorithm

Putting (61) into (60) and applying the matrix inversion Lemma [22] to the big matrix enclosed by the square brackets in the second term on the right side of (60), we obtain

$$\mathbf{P} - \mathbf{R}\mathbf{B}^{-1}\mathbf{R}^T = \mathbf{Q}_e^{-1} + \left(\frac{\partial\tilde{\mathbf{r}}^o}{\partial\mathbf{c}^o}\right)^T \left[\mathbf{Q}_c + \left(\frac{\partial\tilde{\mathbf{r}}^o}{\partial\mathbf{s}^o}\right)(\hat{\mathbf{Z}} - \mathbf{Y}^T\mathbf{X}^{-1}\mathbf{Y})^{-1} \times \left(\frac{\partial\tilde{\mathbf{r}}^o}{\partial\mathbf{s}^o}\right)^T\right]^{-1} \left(\frac{\partial\tilde{\mathbf{r}}^o}{\partial\mathbf{c}^o}\right). \quad (62)$$

It can be concluded from the above equation that $(\mathbf{P} - \mathbf{R}\mathbf{B}^{-1}\mathbf{R}^T)$ is a positive definite matrix because $\mathbf{Q}_e^{-1}$ is positive definite. Note that $\mathbf{P} - \mathbf{R}\mathbf{B}^{-1}\mathbf{R}^T - \mathbf{Q}_e^{-1}$ is also positive definite, because the second term alone in (62) is positive definite due to its symmetric structure as well as the matrix $(\partial\tilde{\mathbf{r}}^o/\partial\mathbf{c}^o)$ having full column rank.

APPENDIX IV
PROOF OF (29)

The upper left three-by-three block of (28) is cov$(\check{\mathbf{u}})$. We shall first evaluate the matrices $(\bar{\mathbf{G}}^T\mathbf{W}^{-1}\bar{\mathbf{G}})$ and

$(\bar{\mathbf{G}}^T\mathbf{W}^{-1}\mathbf{M}\mathbf{W}^{-1}\bar{\mathbf{G}})$ in (28). Substituting the definitions of $\bar{\mathbf{G}}$, $\mathbf{W}$ and $\mathbf{M}$ given in (22), (17) and (27), and using (8) for simplifying the notations, we have

$$\bar{\mathbf{G}}^T\mathbf{W}^{-1}\bar{\mathbf{G}} = \begin{bmatrix} \mathbf{X} & \mathbf{Y} \\ \mathbf{Y}^T & \mathbf{Z} \end{bmatrix} \tag{63}$$

$$\bar{\mathbf{G}}^T\mathbf{W}^{-1}\mathbf{M}\mathbf{W}^{-1}\bar{\mathbf{G}} = \mathrm{diag}[\mathbf{O}_{3\times 3}, \mathbf{R}^T\mathbf{Q}_e\mathbf{R}]. \tag{64}$$

Applying the partitioned matrix inversion formula [22] to $(\bar{\mathbf{G}}^T\mathbf{W}^{-1}\bar{\mathbf{G}})^{-1}$, putting the result together with (64) back to (28) and simplifying yield the upper three-by-three block

$$\mathrm{cov}(\check{\mathbf{u}}) = (\mathbf{X} - \mathbf{Y}\mathbf{Z}^{-1}\mathbf{Y}^T)^{-1} + \mathbf{X}^{-1}\mathbf{Y}\mathbf{B}^{-1}\mathbf{R}^T\mathbf{Q}_e\mathbf{R}\mathbf{B}^{-1}\mathbf{Y}^T\mathbf{X}^{-1}. \tag{65}$$

where $\mathbf{B} = (\mathbf{Z} - \mathbf{Y}^T\mathbf{X}^{-1}\mathbf{Y})$ as is defined under (12). Expanding $(\mathbf{X}-\mathbf{Y}\mathbf{Z}^{-1}\mathbf{Y}^T)^{-1}$ using the matrix inversion Lemma [22] and comparing with $\mathrm{CRLB}(\mathbf{u}^o)_{c^o}$ given in (11) indicate that $(\mathbf{X} - \mathbf{Y}\mathbf{Z}^{-1}\mathbf{Y}^T)^{-1} = \mathrm{CRLB}(\mathbf{u}^o)_{c^o}$. Hence, we have the result (29).

Appendix V
Proof of (53)

By comparing the definitions of $\mathbf{G}_e$ and $(\partial\check{\mathbf{r}}^o/\partial\mathbf{c}^o)$ given in (37b) and (9c), in order to prove (53) is true, we only need to show $\boldsymbol{\rho}_{\mathbf{c},\mathbf{s}_i} \simeq \boldsymbol{\rho}_{\mathbf{c}^o,\mathbf{s}_i^o}$, $i = 1,2,\ldots,M$. Substituting (52) that is valid under C1) and applying the error models (1) and (2), we can express the unit vector $\boldsymbol{\rho}_{\mathbf{c},\mathbf{s}_i}$ as

$$\boldsymbol{\rho}_{\mathbf{c},\mathbf{s}_i} = \frac{\mathbf{c}-\mathbf{s}_i}{\|\mathbf{c}-\mathbf{s}_i\|} \simeq \frac{\mathbf{c}^o-\mathbf{s}_i^o}{\|\mathbf{c}^o-\mathbf{s}_i^o\|} + \frac{\mathbf{e}-\boldsymbol{\Psi}_i}{\|\mathbf{c}^o-\mathbf{s}_i^o\|} \simeq \boldsymbol{\rho}_{\mathbf{c}^o,\mathbf{s}_i^o} \tag{66}$$

where the condition C1) is used again in the second approximation. Hence, the proof of (53) is established.

Acknowledgment

The authors would like to thank the anonymous reviewers for their valuable comments and suggestions which have greatly improved the quality of the manuscript.

References

[1] G. C. Carter, "Time delay estimation for passive sonar signal processing," *IEEE Trans. Acoust., Speech, Signal Process.*, vol. ASSP-29, pp. 462–470, Jun. 1981.
[2] E. Weinstein, "Optimal source localization and tracking from passive array measurements," *IEEE Trans. Acoust., Speech, Signal Process.*, vol. ASSP-30, pp. 69–76, Feb. 1982.
[3] R. Kozick and B. Sadler, "Source localization with distributed sensor arrays and partial spatial coherence," *IEEE Trans. Signal Process.*, vol. 52, no. 3, pp. 601–616, Mar. 2004.
[4] N. Patwari, J. N. Ash, S. Kyperountas, A. O. Hero III, R. L. Moses, and N. S. Correal, "Locating the nodes," *IEEE Signal Process. Mag.*, vol. 22, pp. 54–69, Jul. 2005.
[5] S. Gezici, T. Zhi, G. Giannakis, H. Kobayashi, A. Molisch, H. Poor, and Z. Sahinoglu, "Localization via ultra-wideband radios: A look at positioning aspects for future sensor networks," *IEEE Signal Process. Mag.*, vol. 22, pp. 70–84, Jul. 2005.
[6] T. Li, A. Ekpenyong, and Y.-F. Huang, "Source localization and tracking using distributed asynchronous sensors," *IEEE Trans. Signal Process.*, vol. 54, no. 10, pp. 3991–4003, Oct. 2006.
[7] K. C. Ho and M. Sun, "An accurate algebraic closed-form solution for energy-based source localization," *IEEE Trans. Audio, Speech, Lang. Process.*, vol. 15, pp. 2542–2550, Nov. 2007.
[8] W. H. Foy, "Position-location solution by Taylor-series estimation," *IEEE Trans. Aerosp. Electron. Syst.*, vol. AES-12, pp. 187–194, Mar. 1976.
[9] D. J. Torrieri, "Statistical theory of passive location systems," *IEEE Trans. Aerosp. Electron. Syst.*, vol. AES-20, pp. 183–198, Mar. 1984.
[10] D. Carevic, "Automatic estimation of multiple target positions and velocities using passive TDOA measurements of transients," *IEEE Trans. Signal Process.*, vol. 55, no. 2, pp. 424–436, Feb. 2007.
[11] J. O. Smith and J. S. Abel, "Closed-form least-squares source location estimation from range-difference measurements," *IEEE Trans. Acoust., Speech, Signal Process.*, vol. ASSP-35, pp. 1661–1669, Dec. 1987.
[12] H. C. Schau and A. Z. Robinson, "Passive source localization employing intersecting spherical surfaces from time-of-arrival differences," *IEEE Trans. Acoust., Speech, Signal Process.*, vol. ASSP-35, pp. 1223–1225, Aug. 1987.
[13] B. Friedlander, "A passive localization algorithm and its accuracy analysis," *IEEE J. Ocean. Eng.*, vol. OE-12, pp. 234–245, Jan. 1987.
[14] B. T. Fang, "Simple solutions for hyperbolic and related position fixes," *IEEE Trans. Aerosp. Electron. Syst.*, vol. AES-26, pp. 748–753, Mar. 1990.
[15] J. S. Abel, "A divide and conquer approach to least-squares estimation," *IEEE Trans. Aerosp. Electron. Syst.*, vol. AES-26, pp. 423–427, Mar. 1990.
[16] Y. T. Chan and K. C. Ho, "A simple and efficient estimator for hyperbolic location," *IEEE Trans. Signal Process.*, vol. 42, pp. 1905–1915, Aug. 1994.
[17] K. C. Ho, X. Lu, and L. Kovavisaruch, "Source localization using TDOA and FDOA measurements in the presence of receiver location errors: Analysis and solution," *IEEE Trans. Signal Process.*, vol. 55, no. 2, pp. 684–696, Feb. 2007.
[18] K. C. Ho and L. Yang, "On the use of a calibration emitter for source localization in the presence of sensor position uncertainty," *IEEE Trans. Signal Process.*, vol. 56, no. 12, pp. 5758–5772, Dec. 2008.
[19] R. Moses and R. Patterson, "Self-calibration of sensor networks," in *Proc. SPIE, Unattended Ground Sensor Technologies Applications IV*, Orlando, FL, Apr. 2002, vol. 4743, pp. 108–119.
[20] R. Moses, D. Krishnamurthy, and R. Patterson, "A self-localization method for wireless sensor network," *EURASIP J. Appl. Signal Process.*, vol. 4, pp. 348–358, Mar. 2003.
[21] S. M. Kay, *Fundamentals of Statistical Signal Processing, Estimation Theory*. Englewood Cliffs, NJ: Prentice-Hall, 1993.
[22] L. L. Scharf, *Statistical Signal Processing, Detection, Estimation and Time Series Analysis*. Reading, MA: Addison-Wesley, 1991.
[23] Y. Rockah and P. M. Schultheiss, "Array shape calibration using sources in unknown location, Part I: Far-field source," *IEEE Trans. Acoust., Speech, Signal Process.*, vol. ASSP-35, pp. 286–299, Mar. 1987.
[24] J. C. Chen, R. E. Hudson, and K. Yao, "Maximum-likelihood source localization and unknown sensor location estimation for wideband signals in the near field," *IEEE Trans. Signal Process.*, vol. 50, no. 8, pp. 1843–1854, Aug. 2002.

Le Yang (S'08) was born in Sichuan, China, on June 18, 1979. He received the B.Eng. (with hons.) and M.Sc. degrees in electrical engineering from the University of Electronic Science and Technology of China (UESTC), Chengdu, China, in 2000 and 2003, respectively.

He is currently working towards the Ph.D. degree at the University of Missouri, Columbia. Between 2003 and 2004, he was a Lecturer at the UESTC. From 2004 to 2005, he was with the University of Victoria, Victoria, BC, Canada, working on diversity techniques and performance evaluation of communication systems. In January 2006, he transferred to McMaster University, Hamilton, ON, Canada, where he focused his research on artificial neural networks and computational neuroscience. Since January 2007, he has been with the University of Missouri, Columbia. His current research interests include sensor networks, passive localization, tracking, and signal detection.

K. C. Ho (S'89–M'91–SM'00–F'09) was born in Hong Kong. He received the B.Sc. degree (with First-Class Hons.) in electronics in 1988 and the Ph.D. degree in electronic engineering in 1991, both from the Chinese University of Hong Kong.

He was a Research Associate in the Royal Military College of Canada from 1991 to 1994. He joined the Bell-Northern Research, Montreal, QC, Canada, in 1995 as a Member of Scientific Staff. He was a faculty member in the Department of Electrical Engineering at the University of Saskatchewan, Saskatoon, Canada, from September 1996 to August 1997. Since September 1997, he has been with the University of Missouri, Columbia, where he is currently a Professor in the Electrical and Computer Engineering Department. His research interests are in statistical signal processing, source localization, subsurface object detection, wireless communications, and the development of efficient adaptive signal processing algorithms for various applications, including landmine detection and echo cancellation. He has been active in the development of the ITU-T Standard Recommendation G.168 since 1995. He is the Rapporteur of ITU-T Q15/SG16: Voice Gateway Signal Processing Functions and Circuit Multiplication Equipment/Systems. He is the editor of the ITU-T Standard Recommendations G.160: Voice Enhancement Devices, G.168: Digital Network Echo Cancellers, and G.799.2: Mechanism for Dynamic Coordination of Signal Processing Functions. He is an inventor of three United States patents, three Canadian patents, two patents in Europe and four patents in Asia on mobile communications and signal processing.

Dr. Ho has been serving his second term as an Associate Editor of the IEEE TRANSACTIONS ON SIGNAL PROCESSING since January 2009. He was an Associate Editor of the IEEE TRANSACTIONS ON SIGNAL PROCESSING from 2003 to 2006 and the IEEE SIGNAL PROCESSING LETTERS from 2004 to 2008. He received the Junior Faculty Research Award in 2003 and the Senior Faculty Research Award in 2009 from the College of Engineering of the University of Missouri, Columbia.